Valence-shell ionization of acetyl cyanide: simulation of the photoelectron and infra-red spectra

Stéphane Carniato

Valence-shell ionization of Acetyl cyanide: simulation of the photoelectron and infra-red spectra

Stéphane Carniato[a*]
[a] *Laboratoire de Chimie Physique, Matière et Rayonnement, UMR 7614, Sorbonne Université, 4, Place Jussieu , 75231 Paris Cedex 05 France*
(Dated: January 11, 2023)

The vibrational envelopes of the first and second lines of the acetyl cyanide valence photoelectron spectrum [Katsumata et al., J. of . Elect. Spectr. and Rel. Phenom. 49, 113 (2000)] in gas phase have been simulated considering Taylor expansion of the dipole moment from zero up to second order as well as the changes of geometries/frequencies/normal modes between the initial neutral electronic ground state and the final ($15a'^{(-1)}$, $3a''^{(-1)}$) cationic states. It is shown that the vibrational profile of the first band (A') extending over 3500 cm^{-1} with a vibrational spacing 500 cm^{-1} is not due solely to the overtones (v=0→v'=1,2,3,..) of the C-C=O bending mode as previously suggested but results from a collection of (v=0→v'=1) transitions with frequencies multiple of 500 cm^{-1} associated to stretching C=O at 1550 cm^{-1}, stretching C-C at 1045 cm^{-1}) and C-C=O, C-C≡N bending modes at 370/500 cm^{-1} completed by combination bands. Our calculations also reveal that the structureless and asymmetric shape of the second band (A") is due to activation of the torsion mode with low-frequency (ω≈150 cm^{-1}) induced by rotation (60 degrees) of the methyl group blurring the main vibrational progression (ω≈1115 cm^{-1}) corresponding to cooperative motions of the methyl CH bending and C-C=O bending/C=O stretching. Infra-red spectra of the fundamental and both the $15a'^{-1}$ and $3a''^{(-1)}$ cationic states were finally simulated. Contrary to the photoemission spectra, the infrared intensity of CO stretching motion is very weak. The spectra are mainly dominated by the v=0→v=1 transition of the stretching C≡N and the CH symmetric bending/stretching modes, providing complementary informations between photoemission and Infra-red spectroscopies to capture the nature of the cationic states in acetyl-cyanide.

I. INTRODUCTION

Progress in astrophysical observation offers new areas of investigation for the detection of many and more and more complex molecules in the interstellar medium (ISM). To date, more than 200 different molecules have been detected and 1/3 of them contain more than 6 atoms (see Refs.[1, 2] and references therein). Most of the molecules detected so far are organic. Their observation is particularly relevant since they can be used as sensitive tools to interpret astrophysical processes such as accretion of matter in young stellar objects or plasma jets, complex chemical species giving us insight into the relationship between molecular clouds and planetary formation systems embedded in these clouds.
Light-induced phenomena play determinant roles in routing relative abundances and dynamics of different chemical species taking place in chemical/biological systems or in many astrophysical plasmas. In particular the composition of the molecular gases in ISM is continually evolving due to interactions with electromagnetic fields producing highly reactive neutral or ionized atomic and molecular fragments [3–5]. Most of these atomic or molecular identifications can be accomplished by comparison of recorded spectra on earth to observations of interstellar medium. Consequently, the determination of the physical/chemical properties as well as the understanding of the various reaction paths of these of these atomic/chemical species in space [6, 7] request laboratory measurements assisted by numerical models. Within this framework, infra-red and photoemission spectroscopies are precisely ones of the well-known techniques to explore the structure of matter. They are applied in many fields of research like biology [8, 9], chemistry[10, 11], physics[12, 13] and of course astrophysics [14–16] covering studies in laboratory high-density laser plasmas, hot plasmas of stellar coronae, interstellar clouds [17, 18], and protoplanetary disks of stars [19–21]. Therefore considerable progress has been made over the last three decades in developing experimental approaches towards the investigation of valence (see Ref.[22] and references therein) or inner shell (see Ref.[23] and references therein) resonances and photoionization cross sections for atomic or molecular systems.

Nevertheless, several molecular compounds playing very probably a key role in complex mechanisms[24] are still not well characterized in laboratory for their definitive identification in interstellar media. Furthermore, some interpretations may be controversial and in this context theoretical simulations for band assignments play a crucial role for the analysis of spectroscopic plasma observations and are essential to guide efficiently the analysis of experimental results.

Here, our study concerns ionization in the 11-14 eV energy range of the neutral closed-shell acetyl cyanide system (H_3CCOCN, also called pyruvonitrile, AC) by removing one electron from the two highest doubly occupied molecular orbitals to form the $[CH_3COC{\equiv}N]^+$ cation. This photon energy domain is particularly interesting since it is at the frontier between the regions denoted HI and HII of the ISM. HI region is a cloud in the

*Email:stephane.carniato@sorbonne-university.fr

interstellar medium composed of neutral atomic hydrogen (HI). HI is generally limited to photon energies below 13.6 eV, so only valence excitations of hydrogen atoms or photoionization of molecules and ions with ionization potentials <13.6 eV are relevant. The HII domain is a region of atomic hydrogen ionized by UV (h$\nu \geq$13.6eV) photons from the star atmospheres and is typically a cloud of partially ionized gas in which star formation takes place.

Acetyl cyanide is a precursor of the glycine amino-acid with NH_2CH_2COOH chemical formula. Although it is highly expected to exist in space, it has not been detected yet. However, some related compound aminoacetonitrile (H_2NCH_2CN or AAN), a direct precursor of glycine as well, was identified[25] in Sgr B2(N) in 2008. It is worth noting that both AC and AAN can be formed by Strecker-type[26] reactions (i.e., reactions between an aldehyde or a ketone, HCN, and NH_3 to form amino acids) or through the hydrolysis of cyanoacetylene. These different pathways are thought to be a solid scenario for the formation of amino acids in space. These assumptions are furthermore supported by the detection in the ISM of several chemical compounds involved in the Strecker reaction in addition to AC and AAN (e.g., formamide[27] and formyl cyanide[28]). Photochemically acetyl-cyanide molecule is also an interesting system where laser induced photodissociation of CH_3COCN to form CH_3CO + CN has been extensively explored [29, 30].
The HeI photoelectron spectrum of acetyl cyanide in gas phase has been recorded by Katsumata and co-workers [31] at the end of the nineties. The single photoionization of gas-phase acetyl cyanide and the fragmentation pathways of the resulting cation have been more recently revisited combining theoretical and experimental investigations where the stable forms of the parent, the transition states connecting these minimal structures and the corresponding fragmentation pathways have been successfully characterized (see [24, 32] and references therein). The HeI photoelectron spectrum of acetyl cyanide consists in several ionization bands in the region 11-19 eV. The ionization of the $CH_3CO{\equiv}CN$ molecular system in the outermost doubly occupied $15a'$ orbital gives rise to a photoelectron band ranged between 11-12 eV with a maximum observed at 11.21 eV and a structured vibrational progression extending over 3500 cm^{-1}. Katsumata et al. evaluated the structure of the electronic ground state of AC and of the lowest electronic excited states of AC^+ at the Møller-Plesset (MP2)/6-31G(d) level in order to suggest an assignment of the various lines in this region.

From their MP2 calculations the authors conclude that the structure of the first band is rather consistent with a substantial change in the optimized structure due the CCO bending motion with a vibrational spacing 525 cm^{-1} in the higher energy region extending over 3500 cm^{-1}. It is also claimed by the authors that the first adiabatic and vertical ionization are identical to each other, namely I_a=I_v=11.21 eV. More recently, using the standard coupled cluster approach with perturbative treatment of triple excitations in connection with the aug-cc-pVDZ basis set (i.e., (R)CCSD(T)/aug-cc-pVDZ level) Bellili et al. [24] have estimated at 11.21 eV the adiabatic ionization energy (AIE, i.e. 0-0 transition) of the CH_3COCN^+ cation obtained from ejection of one electron from the 15a' highest doubly occupied molecular orbital (HOMO). According to the authors this value is found nearly equal to the vertical IE (VIE) of AC where the value of the maximum of the peak is confirmed near 11.20 eV using Photoelectron Photo-ion Coincidence (PEPICO) measurements.

As far as we know if geometries and fundamental frequencies of AC and AC^+ have been extensively discussed in the literature [24, 31, 32], simulation and interpretation of the valence photoelectron spectrum have not been so far realized. In the present work, we focused on the nature of the two first bands in the photoelectron spectrum. The interest here lies in the fact that the bands present very different shapes, with vibrational discrete lines for the former, while the second band is an asymmetric broad peak. For that, we have considered different approaches to calculate the Franck-Condon factors considering changes of geometries, frequencies and normal modes for both the neutral AC and AC^+ cation for the assignments of lines in the photoelectron spectra. The specificities of the various models will be discussed in details.

We will first characterize the ground properties of the neutral acetyl cyanide and of their cationic states (A', A"). The computations have been carried out using both standard *ab-initio* approaches (MP2 and DFT). For the first band we will show that changes of geometry upon ionization involved many other different modes than the CCO bending motion. We will show how this apparent vibrational spacing of 500 cm^{-1} which is responsible of the wide vibrational progression extending over 3500 cm^{-1} is, in fact, due to fortuitous combination of different harmonic of vibrational modes and combination bands. For the second band, we will discuss the origin of the broad peak through effect of rotation of the methyl group. Finally, simulation of the neutral and cationic states infra-red spectra will be performed and differences between IR and photoelectron activated bands will be discussed.

II. COMPUTATIONAL DETAILS

As well established in Ref. [24], the electronic wavefunctions of the AC isomers and cations are dominated by a single determinant. Therefore, single-reference methods, like perturbative Hartree-Fock+Møller-Plesset at different n-order (HF+$MP_{n=2,3,..}$), coupled-cluster (CC) or even DFT approaches, are suitable for describing the electronic structure of these species. In Ref. [24], for both neutral and cationic species, the stationary points on the potential energy surface (PES) were characterized using the second-order Møller-Plesset perturbation theory (MP2)[39] and the explicitly correlated CC singles, doubles, and perturbative triples approach (CCSD(T)-F12) [41–44], in conjunction with triple-zeta and double-zeta quality basis sets, respectively (see Ref. [41] and details therein). In the present work, for all minima located on the PESs, structural, energetic, and spectro-

scopic characterization has been performed at MP2 and DFT/B3LYP levels of theory.

A. Vibrational analysis

The study concerns the ionization of the ^{1}A' (Cs symmetry point group) neutral closed-shell acetyl cyanide monomer in gas phase where one electron is removed either from the 15 a' highest (doubly) occupied molecular orbital (HOMO) to form the 15 a'$^{-1}$ doublet ^{2}A' cation or from the (HOMO-1) to form the 3a"$^{(-1)}$ (^{2}A") final state.

The cross-section σ(v',v) of the vibronic transition between the initial electronic state (denoted o) and the final electronic state (denoted f) is considered to be proportional to the square of the transition dipole matrix element:

$$\sigma(v',v) \propto |\langle \Psi_{v'}^{(f)} | \mu | \Psi_{v}^{(o)} \rangle|^2 \quad (1)$$

where $|\Psi_v^{(o)}\rangle$ and $|\Psi_{v'}^{(f)}\rangle$ are the vibronic wave-functions, μ=μ_o+$\sum_{i=1}^{3N-6}[\frac{\partial \mu}{\partial Q_i}]_{Q_i=Q_{i,o}}$ (Q_i-$Q_{o,i}$)+$\frac{1}{2!}$ $\sum_{i=1}^{3N-6}\sum_{j=1}^{3N-6}[\frac{\partial \mu^2}{\partial Q_i \partial Q_j}]$ (Q_i-$Q_{o,i}$)(Q_j-$Q_{o,j}$)+.... is the dipole moment operator, μ_o is the dipole moment of the molecule at the equilibrium geometry, Q_i are the normal modes, $\frac{\partial \mu}{\partial Q_i}$ ($\frac{\partial \mu^2}{\partial Q_i \partial Q_j}$) is the first (second) derivative of the dipole moment with respect to a deformation along the Q_i ($Q_{i,j}$) mode(s) and v(v_1, v_2 . . .)/v'= (v'$_1$, v'$_2$ . . .) are the 3N-6 vibrational modes in the initial (o) and final (f) electronic states. The data have been modeled considering normal modes and frequencies for the initial neutral state and the final cation state, respectively. In first approximation, we assumed that the dipole moment is reduced to its zero order expression, e.g. $\mu \approx \mu_o$, such that σ(v',v) is restricted to the calculation of the overlap $< \Psi_{v'}^{(f)} | \Psi_v^{(o)} >$ matrix elements. These terms were calculated assuming that the ground state vibrational wave-function is written as a product of 3N-6 independent vibrational wave-functions (N is the number of atoms in the non linear molecule),

$$\Psi_v^{(o)}(\mathbf{R}) = \prod_{k=1}^{3N-6} \chi_{v_k}(Q_k - Q_{o,k}^e; \omega_k) \quad (2)$$

where $\chi_{v_k}(Q_k - Q_{o,k}^e; \omega_k)$ is a normalized eigenfunction of an harmonic oscillator of reduced mass μ_k centered at $Q_{o,k}^e$ in a vibrational quantum number v_k undergoing vibration along the coordinate Q_k with frequency ω_k.
For the final state, each lth normal mode of the final state (f) with frequency ω'_l is considered displaced (minimum at Q'$^e_{f,l}$) from the ground state equilibrium position (minimum at $Q_{f,l}^e$) and the vibrational wave-function is written as a product of 3N-6 vibrational wave-functions,

$$\Psi_{v'}^{(f)}(\mathbf{R}') = \prod_{l=1}^{3N-6} \chi_{v'_l}(Q'_l - Q'^e_{f,l}; \omega'_l) \quad (3)$$

If it can be assumed as a crude approximation that frequencies and normal modes are unchanged between the initial and final state, of course, the geometry, normal modes and vibrational frequencies can reasonably differ. The normal coordinates of different electronic states differ as they have different force constants. Thus electronic transitions can cause the normal modes of one electronic state to be rotated or mixed in the normal mode basis of the initial electronic state, a phenomenon first considered by Duschinsky [33] when extending the Franck-Condon principle from di-atomics to polyatomic molecules. It complicates the evaluation of multidimensional Franck-Condon problem as it prevents these integrals from being reduced to simple products of one-dimensional integrals. As suggested by Duschinsky the two sets of normal coordinates are related to each other by a linear transformation, so-called the Duschinsky transformation involving a matrix and a displacement vector. The vector gives the displacement between the equilibrium structures of the two states in terms of the initial state normal coordinates and the matrix can be viewed as an overlap matrix between the normal modes of the two electronic states.

In order to estimate the rotation of the normal modes in the final state, each lth normal mode of the cation are projected over the initial normal modes (denoted j) of the electronic ground state

$$|Q'_l> = \sum_{j=1}^{3N-6} \alpha_{l,j} |Q_j> \quad (4)$$

where

$$\alpha_{l,j} = \sum_{n=1}^{3N} < t'_{l,n} | t_{j,n} > m_n \quad (5)$$

Here $t_{j,n}$=$\frac{x_{j,n}}{\sqrt{m_n}}$(t'$_{l,n}$=$\frac{x'_{l,n}}{\sqrt{m_n}}$) are outputs of the GAMESS(US) software where $x_{j,n}$ (x'$_{l,n}$) and m_n are the n*th* cartesian and mass components respectively of the normalized normal mode j (l) such that,

$$\sum_{j=1}^{3N-6} \alpha_{l,j}^2 = 1 \quad (6)$$

A one-to-one bijective correspondence (see Fig.1, top panel) between each of the 3N-6 modes (denoted v') in the final state and the 3N-6 modes (denoted v) in the initial state can be assumed as a good approximation in case of weak rotations between modes. A surjective (see Fig.1, bottom panel) 3N-6 dimensional relationships between the initial and the final vibrational modes would make more sense for large rotations.

Hence, the expression (1) can be written as the following product:

$$\sigma(v',v) \propto | \prod_{l=1}^{3N-6} [\sum_{j=1}^{3N-6} \alpha_{l,j} < \chi_{v'_l}(Q_{f,j}^e - Q_{o,j}^e; \omega'_l)] | \prod_{p=1}^{3N-6} \chi_{v_p}(Q_{o,p}^e; \omega_p) > |^2 \quad (7)$$

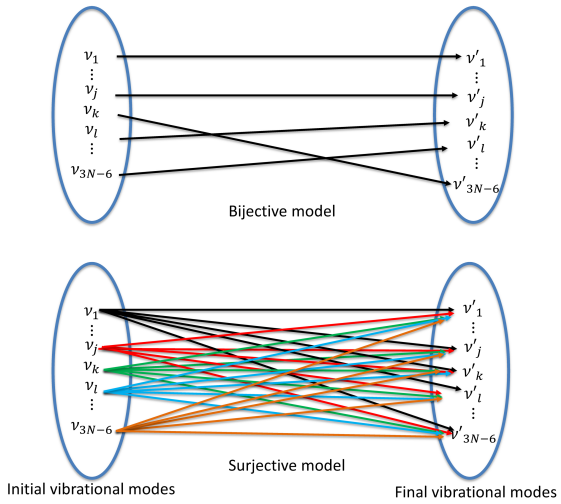

FIG. 1: Bijective (model I) and Surjective (model II) correspondences between the initial and final vibrational modes

and can be reformulated to give

$$\sigma(v',v) \propto |\sum_{i=1}^{3N-6}\sum_{j\neq i}^{3N-6}\sum_{k\neq i,j}^{3N-6}..\sum_{n\neq i,j,k..}^{3N-6}\alpha_{1,i}\alpha_{2,j}\alpha_{3,k}..\alpha_{3N-6,n} < \chi_{v'_i}(Q^e_{f,i}-Q^e_{o,i};\omega'_1)| < \chi_{v'_j}(Q^e_{f,j}-Q^e_{o,j};\omega'_2)| < \chi_{v'_k}(Q^e_{f,k}-Q^e_{o,k};\omega'_3)|...< \chi_{v'_n}(Q^e_{f,n}-Q^e_{o,n};\omega'_n)| \prod_{p=1}^{3N-6}\chi_{v_p}(Q^e_{o,p};\omega_p) > |^2 \quad (8)$$

where each product of the sums runs over 3N-6 terms where non vanishing overlap is restricted between vibrational functions with the same index (ex: $< \chi_{v'_i}(Q^e_{f,i}-Q^e_{o,i};\omega'_{\alpha'(1,2,..3N-6)})|\chi_{v_i}(Q^e_{o,i};\omega_i) >$ but where ω' can take all the final frequencies. In case where a diagonal form is assumed, i.e. $\alpha_{i,j}=\delta_{i,j}$, eq.8 is reduced to a simple (bijective) product of 3N-6 overlaps such as:

$$\sigma(v',v) \propto \prod_{k=1}^{3N-6} | < \chi_{v'_k}(Q^e_{f,k}-Q^e_{o,k};\omega'_k)|\chi_{v_k}(Q^e_{o,k};\omega_k) > |^2 \quad (9)$$

For each term (matrix elements between two vibrational wave-functions) of the product in $\sigma(v',v)$, the analytical approach we have used is based on the overlap between two harmonic oscillators with different frequencies, e.g. ω'_k and ω_k, but similar reduced mass μ_k where v_k and v'_k are the vibrational quantum number for the kth mode in the initial and final states respectively.

Considering the origin of the dipole moment ($\mu\approx\mu_o$), which represents the lowest order nonzero term in a Taylor series expansion, for different frequencies between the neutral (ω_k) and the final state (ω'_k), the calculated analytical FC(ω'_k,v_k;ω_k,0) Franck-Condon factors takes the general expression from the square of the overlap integrals I($\omega'_k, v'_k;\omega_k, v_k$) as derived by Katriel [49]. Numerical values of Franck-Condon factors have then been estimated using the following expression of overlap integrals I_{v_k,v'_k} (square of overlap integrals are called Franck-Condon factors) for every ($\omega'_k, v'_k;\omega_k, v_k$) terms.

$$I(\omega'_k,v'_k;\omega_k,v_k) = (v_k!v'_k!)^{1/2}e^{(-(RS_k)^2\frac{\omega'_k}{\omega'_k+\omega_k})}(\frac{2(\omega'_k\omega_k)^{1/2}}{\omega'_k+\omega_k})^{1/2} \sum_{i_1,i_2,i_3}\frac{1}{i_1!i_2!i_3!(v_k-2i_1-i_3)!(v'_k-2i_2-i_3)!}[\frac{\omega_k-\omega'_k}{2(\omega'_k+\omega_k)}]^{i_1} [\frac{\omega'_k-\omega_k}{2(\omega'_k+\omega_k)}]^{i_2}[\frac{2(\omega'_k\omega_k)^{1/2}}{\omega'_k+\omega_k}]^{i_3}[-2(RS_k)\frac{\omega'_k}{(\omega'_k+\omega_k)}]^{v_k-2i_1-i_3} [2(RS_k)(\frac{\omega'_k}{\omega_k})^{1/2}\frac{\omega_k}{(\omega'_k+\omega_k)}]^{v'_k-2i_2-i_3} \quad (10)$$

where $i_{1,2,3}$, v_k-2i_1-i_3 and v'_k-2i_2-i_3 are all non-negative integers and S_k=$(RS_k)^2$ (RS_k=$\sqrt{\frac{\mu_k\omega_k}{2\hbar}}(Q^e_{f,k}-Q^e_{o,k})$) represents the coupling constant associated to the kth normal mode.

First-order (see support. information, III) Taylor expansion terms of the dipole moment like $< \omega'_k, v'_k|(Q'_k$-$Q'^e_{o,k})|\omega_k, v_k >$ have been also considered. For that we have rearranged the general expression derived by Katriel (see also supporting information, III) for the calculation of dipole-moment integrals expressed in terms of overlap integrals.

Fo the first-order, the general equation takes the form

$$< \omega'_k, v'_k|(Q'_k-Q'^e_{o,k})|\omega_k, v_k >= \frac{1}{\omega+\omega'}\sqrt{\frac{2\hbar}{\mu}} [\sqrt{v'_k\omega'_k}I(\omega'_k,v'_k-1;\omega_k,v_k)+\sqrt{v_k\omega_k}I(\omega'_k,v'_k;\omega_k,v_k-1)] +I(\omega'_k,v'_k,\omega_k,v_k)\frac{\omega'_k(Q'^e_{f,k}-Q'^e_{o,k})}{(\omega'_k+\omega_k)} \quad (11)$$

where I(ω'_k,v'_k -1;ω_k,v_k) and I(ω'_k,v'_k;ω_k,v_k-1) are valid only for $v'_k \geq 1$ and $v_k \geq 1$ respectively.

We have shown (see supporting information, III) that the second-order terms like $| < \phi^{\omega'}_n|(Q-Q_o)^2|\phi^{\omega}_{m=0} > |$ considered here can be expressed in function the first-order $| < \phi^{\omega'}_n|(Q-Q_o)|\phi^{\omega}_{m=1} > |$ terms such as

$$| < \phi^{\omega'}_n|(Q-Q_o)^2|\phi^{\omega}_{m=0} > | = | < \phi^{\omega'}_n|(Q-Q_o)|\phi^{\omega}_{m=1} > |\frac{\sqrt{2}}{2}\sqrt{\frac{\hbar}{\mu\omega}} \quad (12)$$

where

$$| < \phi^{\omega'}_n|(Q-Q_o)|\phi^{\omega}_{m=1} > | = \frac{1}{\omega+\omega'}\sqrt{\frac{2\hbar}{\mu}} [\sqrt{n\omega'}I(\omega',n-1,\omega,1)+\sqrt{\omega}I(\omega',n,\omega,0)] +I(\omega',n,\omega,1)\frac{\omega'(Q_e-Q_o)}{\omega+\omega'} \quad (13)$$

For each mode k, the first derivative $\frac{\partial \mu}{\partial Q_k}_{|(Q_k=Q_{o,k})}$ was calculated using the $Q_{o,k}$(k=1,3N) normal coordinates

$$Q_{o,k} = \frac{1}{\sqrt{\mu_k}} \sum_{l=1}^{3N} t_{k,l}.m_l.x_l \tag{14}$$

where μ_k is the reduced mass associated to the mode k, $t_{k,l}=\frac{a_{k,l}}{\sqrt{m_l}}$ is the lth component of the normal mode k as delivered by the GAMESS(US) package [47], where $a_{k,l}$ is the lth (dimensionless) component of the normal mode k, m_l is the atomic mass associated to the x_l cartesian components (for each atom, similar mass is considered for three cartesians components). Similarly, the cartesian coordinates $x_{o,k}$(k=1,3N) of the molecule at the ground state equilibrium geometry can be developed in function the normal coordinates $Q_{o,l}$(l=1,3N).

$$x_{o,k} = \sum_{l=1}^{3N} t_{l,k}.\sqrt{\mu_l}.Q_{o,l} \tag{15}$$

Assuming a variation $\pm\delta$ along each $Q_{o,j}$ normal mode, the new molecular coordinates (x^{new}) are:

$$x_k^{new}(j,\delta) = x_{o,k} + \delta.t_{j,k}.\sqrt{\mu_j}.Q_{o,j} \tag{16}$$

In order to numerically extract the coupling constants and dipole derivatives (numerical values are reported in supporting information, III and IV), we considered here that the change in geometry between the neutral and final states can be described as a vector $\mathbf{\Delta R}$, whose 3N components are the changes in Cartesian coordinates of the atoms in the molecule (see Ref.[48]). We convert this vector to an equivalent vector, $\mathbf{\Delta R'}$ in mass-weighted coordinates by multiplying each component by the square root of the appropriate mass. This, in turn, can be written as a linear combination of the mass-weighted cartesian coordinates $l_{k,j}$ of the vector l_j, where $l_{k,j}=t_{k,j}m_j$,

$$\mathbf{\Delta R'} = \sum_{k=1}^{3N} \Delta Q_k \mathbf{l_k} \tag{17}$$

where for each one-dimensional ΔQ_k term associated to one normal mode k of the initial state, each component $t_{k,j}=\frac{x_{k,j}}{\sqrt{m_j}}$ of kth normal mode is multiplied by the appropriate atomic mass m_j.

In this case ΔQ_k in length unit can be written as,

$$\delta Q_k = \frac{1}{\sqrt{\mu_k}} \sum_{j=1}^{3N} t_{k,j} m_j (X_f^e(j) - X_o^e(j)) \tag{18}$$

where $X_f^e(j) - X_o^e(j)$ is the difference between the jth cartesian coordinates of the ionic state and the neutral ground state and formula used for S_k is

$$S_k = \frac{\mu_k \omega_k}{2\hbar} \delta Q_k^2 \tag{19}$$

To summarize, in model I (bijective model) one normal mode of the initial state (Q_l^i) is allocated to one normal mode $Q_{l'}^f$ in the final state for which the overlap value between the normal modes (l,l') is the largest one.

This assumption consists to reduce the (3N-6) sum of (3N-6) products in eq.8 to only one product of 3N-6 terms for which $\alpha_{i,k}$ is maximum (for each (i) 3N-6 normal modes in the initial state a k mode is selected (i↔k) for which $\alpha_{i,k}$ is maximum) and residual overlap of interest are $< \chi_{v'_i}(Q^e_{f,i} - Q^e_{o,i}; \omega'_i) | \chi_{v_i}(Q^e_{o,i}; \omega_i) >$ (i=1,...3N-6). The Franck-Condon factors are then calculated using the Katriel expression assuming different set of frequencies for the final state and the initial state. In model II (surjective model), we considered the Katriel expression (eq.10) combined with eq.8 for (3N-6 x 3N-6) Franck-Condon calculations.

All preliminary calculations (geometries, single point energies, vibrational frequencies) were executed using the GAMESS(US) package [47]. The geometries and harmonic frequencies of acetyl cyanide in its neutral electronic ground state and it first (low-lying) cationic states have been calculated at the second-order pertubative møller-plesset (MP2) level of theory and Density functional theory (DFT) approach using the Becke 3-parameter hybrid exchange [45] and the Lee-Yang-Parr gradient-corrected correlation functional [46] (B3LYP). A flexible large correlation consistent polarized valence quadruple zeta (cc-pCVQZ) basis set of Dunning [36] was used for the carbon, nitrogen, oxygen and hydrogen atoms.

In order to compare our simulated profiles with the experimental recorded photoelectron spectra, a gaussian broadening with a full width half maximum fixed at 30 meV was considered. The theoretical spectra were simulated at 0K and room (298 K) temperature.

III. RESULTS AND DISCUSSION

The geometries (distances and bond angles) of the stationary points on potential energy surfaces of AC and AC^+ are listed in Table I. For sake of simplicity, we employed the same labels and notations as in Ref.[31]. The acetyl cyanide molecule is formed by eight (N=8) atoms spatially organized forming a methyl group bonded to a carbonyl group (C=0) itself bonded with a nitrile (C≡N) group moiety. In its neutral initial state (^{1}A') AC belongs to the Cs group of symmetry, where the nitrile and carbonyl functional groups are located in the same plane (see Fig.2). The DFT/B3LYP distances and bond angles are found in very good agreement with the values recently reported by Bellili et al.[32] using post-Hartree Fock (CCSD(T)/MP2) approaches (see Table I). In both cases the calculated r(O-C_2) (1.203 Å/1.203 Å[32]) and r(N-C_3) (1.150 Å/1.157 Å[32]) distances differ significantly from the values (1.224 Å/1.181 Å) established by Katsumata et al. at a RHF/MP2 level of theory. The origin of this net discrepancy is clearly due to the different qualities of basis sets (cc-pCVQZ vs 6-31G(d)) instead of methods (MP2 vs DFT or CCSD(T)). Using a 6-31G(d) basis set the r(O-C_2) (1.211 Å vs 1.162 Å)

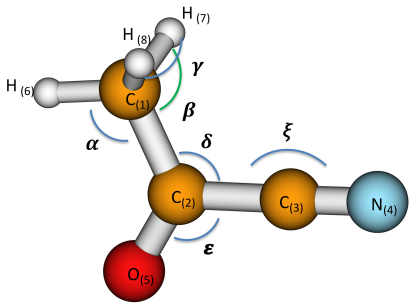

FIG. 2: Geometrical picture of the acetyl cyanide molecule showing atoms (labeled by numbers) and bond angles (Greek letters)

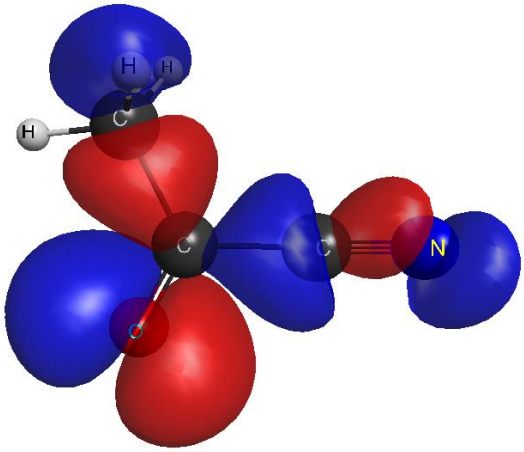

FIG. 3: Electronic density of the (in-plane) highest occupied Molecular orbital (HOMO, 15a') in acetyl cyanide

and r(N-C_3) (1.222 Å vs 1.182 Å) distances calculated at DFT(B3LYP) and MP2 levels (all the occupied/virtual molecular orbitals are considered as active orbitals) notably differ. Using a larger cc-pCVQZ basis set (see Table I) the bond lengths calculated at a RHF/PM2 level of theory are found very similar to the DFT/B3LYP values, except for the r(N-C_3) distance for which a very good agreement is reached between MP2 (1.168 Å) and experiments (1.167 Å) while the DFT nitrile distance (1.150 Å) is still slightly underestimated.

In Table II are reported the DFT/B3LYP/cc-pCVQZ and MP2/cc-pCVQZ harmonic vibrational frequencies calculated in the present work, compared with the best-estimated fundamental frequencies reported by Bellili et al. [32] and the experimental data recorded by Bell et al. [56] for the neutral AC. In details, the so-called "best" harmonic (ω_{best}) frequencies were evaluated by the authors at a CCSD(T)/VTZ level taking into account Complete Basis Set (CBS), core-valence (CV) and effect of diffuse functions in the basis set corrections. Anharmonic corrections ($\Delta\nu$) were then evaluated at the MP2/AVTZ level of theory that is used to derive the best-estimated fundamentals.

As a results, our theoretical (harmonic) values are slightly overestimated in comparison to experimental and anharmonic frequencies. However, the deviation is quite moderate ranging from 30-40 cm^{-1} for modes with frequencies between 1000-2000 cm^{-1} up to 100 cm^{-1} for the modes with higher frequencies (3500 cm^{-1}) .

The average difference (in %) between our calculated values and the experimental data is estimated to 2.6%. The most relevant discrepancy vs experiment is observed for ω_{16} (CO out-of-plane wagging) with the fundamental calculated at ≈596 cm^{-1} while the experimental value is estimated to 535 cm^{-1} by Heise et al.[40].

The difference is here about 60 cm^{-1}, which in relative terms is a discrepancy of 11%. This value is too large compared to the ones obtained for the other transition frequencies and the literature on this topic (see, for example, Ref. [52, 53]). Therefore, as already pointed out in Ref. [32], we confirm that the experimental frequency of 535 cm^{-1} is miss-assigned to ν_5 ; in view of its very low intensity, this band has been attributed instead to a combination band. It is worthwhile noting that in Ref. [40], unassigned transitions at 578 cm^{-1} and 581 cm^{-1} were observed. In these conditions, if we consider the ν_5 fundamental to a mean-value transition at 580 cm^{-1} , the deviation $[\nu_{calc}\text{-}\nu_{exp}]/\nu_{exp}$ (≈2.8%) of the calculated frequency coincides rather well with the average observed-calculated difference which decreases to 2.1% if we substitute ν_{exp} at 535 cm^{-1} by ν_{exp} at 580 cm^{-1}.

The ejection of one electron from the highest (15a') occupied molecular orbital (HOMO) leads to the low-lying (^{2}A') doublet final state of AC^+. The picture displayed in Fig.3 of the highest molecular orbital (HOMO) shows that the electronic density is mostly localized between C_1-C_2, C_2-C_3, C_3-N and the lone pair of the oxygen atom in the carbonyl group.

The free zero-point vibrational (ΔZPE) energy difference (-0.12 eV or 960 cm^{-1}) between the (adiabatic) electronic energy of the $15a^{-1}$ cationic state in its fully optimized geometry (E^+=-245.6384 a.u) and the (vertical) energy (E_{vert}=-245.63399 a.u) of the cation in the initial ground state geometry indicates that only a small gain of energy is achieved when nuclear relaxation. Obviously the Cs molecular symmetry is kept there are few characteristic changes in the equilibrium geometries between the neutral state and the $15a'^{(-1)}$ cation state. As results, the changes of the bond lengths between AC and AC^+ are less than 0.055 Å where the maximum displacement amount to -0.054 Å with a significant shortening of the r(C_2-C_3) chemical bond.

Conversely the r(O-C_2) bond length increases by 0.022 Å (0.018 Å) and the r(N-C_3) distance is lengthened by only 0.005 Å (0.002 Å) at DFT/cc-pCVQZ (MP2/cc-pCVQZ) levels of theory. These different opposite modifications of bond lengths between CO and C_2C_3 is correlated by changes of the bond order indices for the C_2-O (1.74→1.4) and C_2-C_3 chemical bonds (1.049→1.129)

TABLE I: DFT/cc-pCVQZ and MP2/cc-pCVQZ geometries of the neutral ^{1}A' ground state compared to the two first ^{2}A'(15a'$^{(-1)}$) and ^{2}A'(3a"$^{(-1)}$) ionic AC$^+$ final states of acetyl cyanide. Ref.[32]^a: CCSD(T)/VTZ calculations: the valence correlation energy is computed at the coupled-cluster single/double augmented by perturbative treatment of triple excitations (CCSD(T)).Ref.[32]^b: Moller-Plesset (MP2) calculations with valence triple zeta (VTZ) basis set. ω is the dihedral O_5-C_2-C_1-H_6 angle. ^{c} CH bond in the molecular plane. ^{d} CH bonds out-of-the molecular plane.

Parameter	Neutral (AC)						Cation 15a'$^{(-1)}$			Cation 3a"$^{(-1)}$
	DFT/B3LYP	MP2	CCSD(T)/VTZ[32]	MP2/VTZ[32]	MP2/6-31G(d)[31]	Expt[38]	DFT/B3LYP	MP2	Ref.[32]	
r(O_5-C_2)	1.202 8	1.210 0	1.203 3	1.214 2	1.224	1.208	1.224 7 (0.022)	1.228	1.219 8	1.291 2 (0.088)
r(C_2-C_3)	1.483 8	1.477 5	1.482 8	1.479 2	1.482	1.477	1.430 3(-0.054)	1.426	1.433 6	1.425 3(-0.059)
r(N_4-C_3)	1.150 5	1.167 8	1.156 9	1.172 9	1.183	1.167	1.153 6 (0.004)	1.170	1.155 2	1.169 8 (0.020)
r(C_1-C_2)	1.500 5	1.492 5	1.495 6	1.495 5	1.501	1.518	1.505 7 (0.005)	1.484	1.506 1	1.446 8(-0.053)
r(H_6-C_1)^c	1.086 1	1.079 6	1.084 9	1.085 6	1.090	1.116	1.086 2 (0.000)	1.080	1.093 6	1.084 3(-0.002)
r(H_7-C_1)^d	1.091 5	1.084 3	1.089 8	1.090 5	1.095		1.096 5 (0.005)	1.088	1.085 1	1.111 0 (0.019)
α	109.71	109.64			109.1		111.44	111.64	110.98	115.66 (5.95)
β	109.66	109.27			109.9		105.95	106.15		107.74(-1.92)
γ	106.98	107.39			119.1		109.48	108.42		99.64(-7.34)
δ	114.84	114.53			115.3	114.20	122.92	123.34		123.83 (8.99)
ϵ	119.60	119.96	119.66	119.81	119.5		118.81	118.95	118.95	114.53(-5.07)
ζ	178.84	178.27	178.31	178.82	179.9	179.20	177.18	175.35	177.09	177.84(-1.00)
ω	0.00						0.00			53.05

TABLE II: Acetyl cyanide (DFT/B3LYP/cc-pCVQZ) and MP2/cc-pCVQZ calculated vibrational harmonic frequencies of the ground state compared to: ^{a} harmonic frequencies (ω_{best}=ω(CCSD(T)+ω(CBS)+$\omega(CV)$+ω(aug), see Ref.[32] for more details); ^{b} fundamentals ν_{best} determined from ω_{best} harmonic frequencies augmented by anharmonic corrections evaluated at the MP2/AVTZ level anharmonic correction (ν_{best}=ω_{best}-$\Delta\nu$(MP2/AVTZ), see Ref.[32] for more details) and experimental data (values in cm^{-1}). The modes are indexed using the Cs symmetry and decreasing frequency values (in parenthesis are given the numbering following the increasing order of frequencies).

symmetry	mode description	Vibrational frequencies				
		DFT/B3LYP	MP2	ω_{best}^{a}	ω_{best}+anharmonic MP2/VTZ corr.^{b}	Expt.
A"						
ω_{18}(1)	CH_3 torsion	129	136	136	129	126
ω_{17} (3)	out of plane C≡N bend	245	214	247	250	245
ω_{16} (5)	CH_3-C_3-C_2=O out-of-plane wag.	596	581	584	585	535
ω_{15} (9)	CH_3-C=O out-of-plane rock	1049	1058	1046	1018	1026
ω_{14}(13)	CH_3 antisymmetric bend	1468	1493	1477	1437	1432
ω_{13}(17)	CH_3 antisymmetric stretch	3086	3180	3120	3002	2976
A'						
ω_{12} (2)	C-C≡N in plane bend	177	160	175	175	176
ω_{11} (4)	C-C-C bend + C_1-C_2=O bend	437	433	429	428	431
ω_{10} (6)	C-C≡N bend +C_3-C_2=O bend	599	585	592	596	589
ω_9 (7)	C_2-C_3 stretch + C_1-C_2 stretch + H_3C-C_2=O bend	715	730	719	715	712
ω_8 (8)	CH_3 in-plane rock + C_1C_2 stretch + C_3-C=O bend	985	1003	989	971	976
ω_7 (10)	CH_3 rock +CC=O bend +$C_2C_{1,3}$ stretch	1193	1217	1205	1178	1178
ω_6 (11)	CH_3 symmetric bend + C_1C_2 stretch	1398	1398	1398	1355	1368
ω_5 (12)	CH_3 antisymmetric bend	1458	1485	1469	1422	1428
ω_4 (14)	C=O stretch	1776	1735	1779	1775	1740
ω_3 (15)	C≡N stretch	2323	2163	2256	2252	2229
ω_2 (16)	CH_3 sym. stretch	3031	3099	3047	2955	2933
ω_1 (18)	CH_3 antisymmetric stretch	3146	3229	3169	3046	3027

between the neutral and the cation indicating that electronic density decreases between carbon and oxygen while it increases between carbons. The opposite changes of the C_2C_3 and the C-O interatomic distances while the C_1C_2 bond length is unchanged is also concomitant with a significant increase of the (δ) angle by ≈8 degrees between the three carbons atoms while ϵ remains equal to its initial value (≈119 degrees).

The calculated vibrational frequencies for the ^{2}A' final doublet state are reported in Table III. For each normal mode of AC$^+$ are indicated the square of the coefficients corresponding to the projections of the cation normal modes onto those of the neutral ground state.

As observed, except for modes with low ($\omega'_{18-12-17-16-11-10-9}$) and high frequencies ($\omega'_{3,2,1,13}$) for which the projection is maximum along the diagonal (bijective behavior), the rest of modes ranging between 900 cm^{-1} and 1550 cm^{-1} in AC$^+$ present significant

transformations in the final state compared to the vibrational modes in the neutral ground state. With the increase of the r(O-C_2) bond in AC^+, the frequency of the CO stretching mode is notably reduced (ω'_4=1551 cm^{-1}) compared to its value (ω_4=1776 cm^{-1}) in the initial state. For the three modes associated to the C_2-C_3 bond stretching, e.g. ω'_9 at 712 cm^{-1}, ω'_7 at 1045 cm^{-1} and ω'_6 at 1306 cm^{-1} (each mode is significantly expanded over ω_8, ω_7, ω_6 and ω_5), the corresponding frequencies are found significantly different compared to those calculated for AC in its neutral electronic configuration. This could be explained by the fact that the C_2-C_3 bond stretching motion in ^{2}A' is coupled with other deformations such as ω_8 (CH_3 rocking, 985 cm^{-1}) for ω'_7 and ω_7 (CCO bend + CH_3 rocking, 1193 cm^{-1}) or ω_5 for ω'_6 with lower or intermediate frequencies.

A. Band 15a'$^{(-1)}$: spectral assignments

As reported by Katsumata et al. [31] (see also Fig. S2 in supporting information, I) the spectrum shows a main band at 11.21 eV and a satellite energy region composed by a discrete vibrational progression extending over to nearly 3500 cm^{-1}. It is composed by five well-identified structures separated from each other by a nearly regular vibrational spacing of ≈500 cm^{-1}. As claimed by the authors, the structures would be consistent with a vibrational progression corresponding to the various overtones of the CCO bending motion with 525 cm^{-1} of vibrational frequency from their MP2 calculations.

In order to estimate the theoretical origin of energies for the ^{2}A' photoemission line, we have determined first the adiabatic ionization energy (AIE is the energy difference between the vibrational ground state of the neutral species (v= 0) and that of the positive ion (v' = 0) derived from the (adiabatic) electronic energies of the fully optimized initial and final states corrected by vibrational zero-point energy (ZPE). Ignoring the ZPE correction, the DFT/B3LYP electronic energy difference ($\Delta E=E^+-E^o$) between the fully geometry optimized ^{2}A' and the ^{1}A' adiabatic states is equal to 11.007 eV. Taking into account the zero-point vibrational energy correction (ΔZPE=-0.064 eV), the adiabatic ionization energy AIE is finally estimated to 10.94 eV.

As it can be observed, the value is underestimated with respect to the calculated AIE reported by Bellili et al.[24, 32] (AIE≈11.20 eV) pointing out here the limits of the (harmonic) approach based on DFT to determine very accurately the absolute energy position of the fundamental transition. However, if their value matches perfectly with the maximum of the vibrational progression found at AIE = 11.21 eV by Katsumata et al. [31] using HeI photoelectron spectroscopy as well as the value extracted [24, 32] from Photoelectron Photo-ion Coincidence (PEPICO) spectra of the monomer (11.20 ± 0.01 eV), as reported by the authors the uncertainty of the estimation on their AIE value is not much better than ≈0.1 eV, ranging to nearly 11.20±0.1 eV depending the level of approximations (CCSD(T)/VTZ/ZPE or CCSD(T)/CBS+CV+ZPE levels). The match is thus essentially fortuitous, vitiating any quantitative conclusions obtained by comparing the calculated adiabatic IE with the experimental vertical IE. Furthermore, the energy region of the main peak is not only composed by the (0→0) ionization transition, but contain contributions of low-lying frequency modes fundamental transitions as well as hot-bands due to temperature effects (298 K) likely to slightly move the maximum of the main peak with respect to the AIE value. Thus, for sake of simplicity, the 0→0 ionization transition will be considered as the zero of frequencies. In Fig. 4 are reported the theoretical spectra obtained with models I and II at 0K compared to a pseudo-spectrum reconstructed from special points taken from experimental data recorded by Katsumata et al.[31]. As it can be seen, whatever the model used, the most intense band is well reproduced by theory and is unambiguously assigned to the fundamental 0-0 transition. The simulations reproduce also very well the general appearance of the recorded experimental spectrum where a collection of satellite lines are observed in the 100-3500 cm^{-1} energy range with a monotonic decrease in intensity. In details, the Franck-Condon factors reported in Table III and Fig.4 for models I and II indicate that the satellite region of the spectrum is mainly governed by FC factors associated to 0→1 excitations and bands of combination associated to the $\omega'_{12,11,10,9,8,7,6,4}$ in-plane modes. Assuming a similar area under the experimental and theoretical peaks, the calculated intensity of the main peak is slightly overestimated while intensity of the satellite energy region is fairly well reproduced. We have analyzed below in details the nature of the different components covering the energy domain of the theoretical spectrum.

1. *Region 0-500 cm^{-1}*

The first satellite peak is located very close to the fundamental (0→0) transition and is the contribution of single (0→1) transitions and bands of combination.

The low-lying line contributing to the second peak corresponds to the v=0→v'=1 transition associated to the (a') in-plane C-C≡N bending mode ω'_{12} at 160 cm^{-1}. A second line is related to the (v=0→v'=1) transition associated to the in-plane C-C=O bending mode ω'_{11} at 325 cm^{-1} mainly contributing to the experimental shoulder observed at 350 cm^{-1}. Close to 500 cm^{-1} from the (0→0) fundamental transition, the $\omega'_{12}+\omega'_{11}$ band of combination at 487 cm^{-1} involving the CCN and CCO in-plane bending motions as well as to FC(0→1) factor for the mode ω'_{10} lying at ≈ 496 cm^{-1} are both clearly identified by theory and significantly contribute to the shoulder intensity in the 300-500 cm^{-1} frequency region.

In the energy region between 500-900 cm^{-1} a second rather flat shoulder is also predicted by theory. It is due to the v=0→v'=1 transition for the mode ω'_9, v=0→v'=2 transitions for $\omega'_{11}/\omega'_{10}$ and combination bands such as $\omega'_{12,11}+\omega'_{10}$ and $\omega'_{12}+\omega'_9$. In spite the experimental resolution of the spectrometer considered here (30 meV) this structure is not clearly identified on the experimental spectrum and higher resolution measurements are clearly

TABLE III: Horizontally: Calculated DFT/B3LYP/cc-pCVQZ frequencies of the harmonic vibrational modes (ω) of the initial ground state; Vertically: calculated DFT/B3LYP frequencies of the harmonic vibrational modes of the cationic state and squared coefficients of projection of the normal modes of the cation onto the neutral harmonic vibrational modes are reported. In bold the largest absolute squared overlap coefficient. In red, largest squared overlap coefficient below 0.85. The modes are indexed using the Cs symmetry and decreasing frequency values (in parenthesis are given the numbering following the increasing order of frequencies).

M		ω_{18}	ω_{12}	ω_{17}	ω_{11}	ω_{16}	ω_{10}	ω_9	ω_8	ω_{15}	ω_7	ω_6	ω_5	ω_{14}	ω_4	ω_3	ω_2	ω_{13}	ω_1	Assignment
		129	177	245	437	596	599	715	985	1049	1193	1398	1458	1468	1776	2323	3031	3086	3146	
a”																				
ω'_{18} (1)	118	**0.99**	–	0.01	–	–	–	–	–	–	–	–	–	–	–	–	–	–	–	CH_3 torsion
ω'_{17} (3)	217	0.01	–	**0.99**	–	–	–	–	–	–	–	–	–	–	–	–	–	–	–	out of plane C-C≡N bend
ω'_{16} (6)	563	–	–	–	–	**0.99**	–	–	–	–	–	–	–	–	–	–	–	–	–	C_3-C=O wag.
ω'_{15} (8)	970	–	–	–	–	–	–	–	–	**0.99**	–	–	–	–	–	–	–	–	–	CH_3C=O out-of-plane rock
ω'_{14} (13)	1426	–	–	–	–	–	–	–	–	–	–	–	–	**0.99**	–	–	–	–	–	CH_3 antisym. bend.
ω'_{13} (17)	3052	–	–	–	–	–	–	–	–	–	–	–	–	–	–	–	–	**1.00**		CH_3 antisym. stretch
a’																				
ω'_{12} (2)	161	–	**0.99**	–	–	–	–	–	–	–	–	–	–	–	–	–	–	–	–	-C≡N bend
ω'_{11} (4)	326	–	–	–	**0.83**	–	0.10	0.03	–	–	0.03	–	–	–	–	–	–	–	–	C_1-C_2=O bend
ω'_{10} (5)	496	–	–	–	0.14	–	**0.79**	0.03	0.03	–	0.02	–	–	–	–	–	–	–	–	in plane C-C≡N bend + O=C-C_3 bend
ω'_9 (7)	712	–	–	–	0.01	–	0.02	**0.85**	0.06	–	0.03	0.02	–	–	–	–	–	–	–	(C_2-C_1 +C_2-C_3) stretch
ω'_8 (9)	972	–	–	–	–	–	0.08	0.07	**0.70**	–	0.06	0.05	0.01	–	0.02	–	–	–	–	CH_3 in-plane rock + antisym. C_1C_2/C_2-C_3 stretch
ω'_7 (10)	1045	–	–	–	0.02	–	0.02	–	0.20	–	**0.56**	0.12	0.01	–	0.06	–	–	–	–	CH_3 in-plane rock + antisym. C_1C_2/C_2-C_3 stretch
ω'_6 (11)	1306	–	–	–	–	–	–	–	0.01	–	0.27	**0.51**	0.15	–	0.06	–	–	–	–	CH_3 sym. bend + C_2-C_3 stretch+ C=O stretch
ω'_5 (12)	1393	–	–	–	–	–	–	–	–	–	–	0.17	**0.81**	–	0.01	–	–	–	–	CH_3 antisym. bend
ω'_4 (14)	1551	–	–	–	–	–	–	–	–	–	0.01	0.13	–	–	**0.85**	–	–	–	–	C=O stretch + H_7CH_8 sym. bend
ω'_3 (15)	2318	–	–	–	–	–	–	–	–	–	–	–	–	–	–	**0.99**	–	–	–	C≡N stretch
ω'_2 (16)	2986	–	–	–	–	–	–	–	–	–	–	–	–	–	–	–	**0.98**	–	0.01	CH_3 sym. stretch
ω'_1 (18)	3157	–	–	–	–	–	–	–	–	–	–	–	–	–	–	–	0.01	–	**0.99**	CH_3 antisym. stretch

expected to prove its presence.

2. *Region 1000-1500 cm^{-1}*

The energy position of the broad peak in the region denoted III is measured at nearly 1000 cm^{-1}. Our calculations indicate that this band is mostly due to the contribution of two 0→1 transitions. The largest one corresponds to the mode ω'_7 at 1045 cm^{-1} associated to the C-C=O bend/CH_3 rocking and C_1C_2 stretching motions. A large contribution to the intensity also comes from the mode ω'_9 at 972 cm^{-1}. This mode closely ressembles to ω_8 (overlap=0.7) which corresponds to in-plane CH_3 rocking, C-C=O bending and C_1C_2 stretching motions.

The experimental energy region near 1500 cm^{-1} present two structures (denoted IV and V) separated by nearly 200 cm^{-1}. This double-peak feature is fairly well reproduced by the present calculations. The region denoted (IV) is mostly due to the FC(0→1) factor for the ω'_6 vibrational mode where the frequency is calculated at 1306 cm^{-1} (CH_3 sym. bend + C_2-C_3 stretch+ C=O stretch) with significant contributions of ω'_{11}+ω'_8 and ω'_{11}+ω'_7 bands of combination.

The fifth (V) energy region exhibits an other maximum centered at nearly 1500 cm^{-1}. This peak is unambiguously assigned to the 0→1 transition for the mode ω'_4 at 1550 cm^{-1} associated to the CO stretching motion weakly coupled with the CH_3 symmetric bending and C_1C_2 stretching movement. The energy of this transition is very close to the ω'_{10}+ω'_7 band of combination estimated at 1541 cm^{-1} with weaker intensity.

The identification of the origins of the different bands at 500 cm^{-1}, 1000 cm^{-1} and 1500 cm^{-1} is clearly in contradiction with the interpretation suggested by Katsumata et al. [31] who claimed that the satellite bands are due to overtones of solely the C-C=O bending mode. The reason of this misinterpretation lies essentially in the fact that due to a net increase of the CO bond length the vibrational frequency of the CO stretching mode in the ionized final state decreases significantly (1774 cm^{-1}→1550 cm^{-1}). The frequencies of the modes ω'_7 and ω'_4 contributing to the satellites (III) and (V) respectively are accidentally equal to two and three times the ω'_{10} fundamental frequency, that could explain the fortuitous presence of bands at a multiple of the 500 cm^{-1} frequency and the reason of this wrong assignment [31].

3. *Region 2000-3500 cm^{-1}*

The experimental spectrum shows two additional weak satellite bands (VI and VII) centered at 2000 cm^{-1} and 2500 cm^{-1} respectively. These two regions are also very well reproduced by theory. The lines correspond to a collection of bands of combination ($1\omega'_a$+$1\omega'_b$) involving the vibrational modes $\omega'_{12,11,10,9,8,7,6}$ and ω'_4. The C≡N (mode ω'_3) 0→1 band at 2320 cm^{-1} merges with the bands of combination and is difficult to observe due to its weak intensity. This spectral region 2000-2300 cm^{-1} is yet of special interest since the triple CN bonds of nitriles are relevant to pre-biotic chemistry.

Comparing models I and II, as one can be observed, both the corresponding simulated spectra are found very similar and successfully reproduce the most important features of the experimental spectrum. This is not surprising since a relative one-to-one correspondence exists between most of the ω_i modes in the initial state and ω'_i modes in the final cationic state removing of one electron from the HOMO (see Table III). Only for $\omega'_{10,9,8,7,6,5,4}$

TABLE IV: DFT/B3LYP/cc-pCVQZ harmonic frequencies of the vibrational modes associated to the 15 a'$^{-1}$ ionized state. A : RS values and diagonal ($FC_{0\to n}$(n=1-to-3)) Franck-Condon factors derived from eq.10 for model I.b and II (see text). In bold: most important FC factors (≥ 0.09) contributing to the vibrational profile.

Mode	Frequency (cm^{-1})	RS(k)	$FC_{0\to0}$	$FC_{0\to1}$	$FC_{0\to2}$	$FC_{0\to3}$
a"						
ω'_{18} (1)	118	-0.0004	**0.9989**	–	0.0017	–
ω'_{17} (3)	217	0.0001	**0.9982**	–	0.0018	–
ω'_{16} (6)	563	0.0004	**0.9996**	–	0.0004	–
ν'_{15} (8)	970	-0.0001	**0.9992**	–	0.0008	–
ω'_{14} (13)	1426	-0.0002	**0.9999**	–	0.0001	–
ω'_{13} (17)	3052	0.0000	**0.9999**	–	–	–
a'						
ω'_{12} (2)	161	0.5077	**0.7813**	**0.2009**	0.00173	0.0005
ω'_{11} (4)	326	-0.5834	**0.7397**	**0.2464**	0.0130	0.0005
ω'_{10} (5)	496	0.4225	**0.8469**	**0.1499**	0.0029	0.0003
ω'_{9} (7)	712	0.3965	**0.8548**	**0.1344**	0.0103	0.0005
ω'_{8} (9)	972	0.3548	**0.8825**	**0.1111**	0.0062	0.0002
ω'_{7} (10)	1045	0.4537	**0.8233**	**0.1688**	0.0080	–
ω'_{6} (11)	1306	0.3251	**0.9024**	**0.0953**	0.0023	
ω'_{5} (12)	1393	0.0967	**0.9906**	0.0093	0.0001	–
ω'_{4} (14)	1551	-0.3634	**0.8821**	**0.1160**	0.0018	0.0001
ω'_{3} (15)	2318	-0.1052	**0.9890**	0.0110	0.0005	–
ω'_{2} (16)	2986	-0.0327	**0.9989**	0.0011	–	–
ω'_{1} (18)	3157	-0.0329	**0.9989**	0.0011	–	–

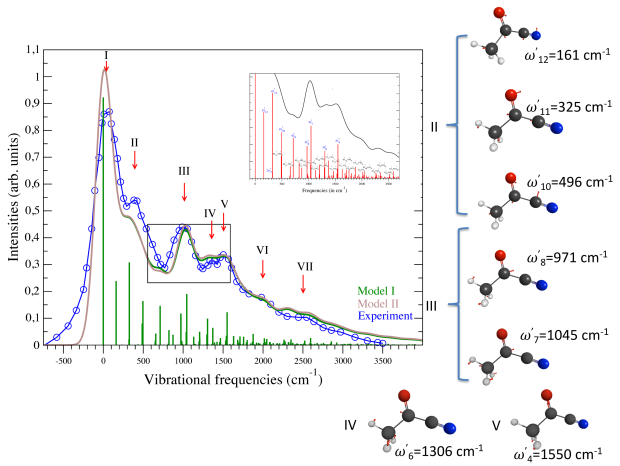

FIG. 4: Simulated spectra of the ^{2}A' ionized state in the region 0-3500 cm^{-1} obtained with bijective (I) and surjective model (II) models at the zero order approximation of the dipole moment. For the model I, intensities and frequencies of the vibrational bands associated to (i,0;i,v') (i=1-to-18; v'=0,1,..4) diagonal Franck-Condon values (see text) are given. The box corresponds to the energy region where surjective/bijective models give different results. Assignments of the most important vibrational bands in the satellite energy region of the 15a'$^{-1}$ photoelectron spectrum are given in the inset (see also supporting information for more details, II). The arrows indicate the positions of the main structures observed experimentally[31] and discussed in the text. Right: The frequencies and corresponding cooperative motions of the atoms of the modes with the largest FC(0→1) factor are displayed

central vibrational modes in the final electronic state ranging between 500 cm^{-1} and 1550 cm^{-1} significant rotations occur. However, in spite rotation effects as described through eq.8, the changes of the intensities in the energy region between 500-1500 cm^{-1} are very small and the bijective approach assuming a one-to-one correspondence between each initial and final vibrational mode is here not so different to the surjective model application.

Regarding the general shape of the theoretical spectrum vs experiment, the intensity of the fundamental (0→0) peak at 0K and zero-order approximation of the dipole operator is largely overestimated compared to the measurements. For instance the calculated intensity ratio between peaks I and III is estimated to $r^{theo}_{I/III}$=2.65 while it is measured to $r^{exp}_{I/III}$=2.0 experimentally. Furthermore as one can be observed on the experimental spectrum the main line presents a long tail in the low-binding energy region far from being well reproduced by theory.

This discrepancy can be due to several effects. In order to finely analyze their contributions, we have reduced the experimental broadening to 25 meV. The intensity of the harmonics associated to ω'_4 is clearly sensitive to a small change of the carboxyl (C=O) bond length. Using model I, we considered (see Fig.5, panel up/left) several deviations of the CO bond distance (-0.003 Å/0.000 Å/+0.003 Å/+0.006 Å) from the DFT/B3LYP calculated value (1.2247 Å). The lengthening of the CO distance in the final state changes substantially the intensity ratio between the peaks lying at 1370 cm^{-1} and 1500 cm^{-1} respectively. The intensity ratio between peaks IV and V is particularly very well reproduced for r_{CO}=1.2277 Å, e.g.

a lengthening of the CO bond by 2.24 pm with respect to the initial neutral geometry.

However, the most important modes (ω'_{12},ω'_{11} ω'_{10}) contributing to the first energy satellite region between 100/500 cm^{-1} and the satellite band ($\omega'_{8,7}$) at 1000 cm^{-1} above the main peak are also very sensitive to the O=CC or O=CCN bending angles and CH_3 (rocking motion) coordinates. Thus the finding of an optimal set of parameters is clearly difficult to reach.

One other explanation is the missing of terms beyond the zero order in the dipole moment expansion. Neglecting the high order corrections could limit the detection of the contributions to the regions I and II of the out-of-plane vibrational modes 118 cm^{-1}/217cm^{-1} and 563 cm^{-1} respectively. However, as displayed in Fig.5 (left/bottom) considering 1st order up to the second order corrections (for the 2nd order, only the diagonal $\sum_{i=1}^{3N} \frac{\partial^2 \mu}{\partial Q_i^2}$ terms have been considered, see support. information, V for numerical data) the intensity ratio between the main line and satellite energy region ($r_{I/III}^{theo}$=2.58) is only weakly changed (see suppl. inform., II) compared to the zero-order approximation.

Other factors like temperature or the nature (form) of the energy background under the photoelectron profile can also be determinant in order to correctly estimate the optimal intensity ratio between the main peak and satellite lines. The nature of the background being unknown a priori here, only temperature effect will be considered below. In Fig.5 (right/up and right/bottom panels) we have reported the simulated spectra at T≈300 K. We assumed that only the four ($\omega_{18-17-12/11-10}$) vibrational modes with lowest frequencies contribute reasonably to the hot bands. Vibrational levels up to v=4-4-4/2-2 were considered, covering 1944 different excited initial vibrational configurations.

As fundamental improvements, the low and high energy tails of the theoretical main peak are broadened due to contribution of the hot bands and a good agreement is reached between theory at 298 K and experimental data [31]. Assuming a similar area under the experimental and theoretical profiles, the calculated intensity ratio between the main peak and satellite energy region is also very well reproduced compared to the simulation at 0K, especially using 1st-order correction of the dipole operator where intensity ratio between the satellite band III and the main peak reaches a value $r_{I/III}^{theo}$=2.18 ($r_{I/III}^{theo}$=2.33 for zero-order approximation) in excellent agreement with the experimental value.

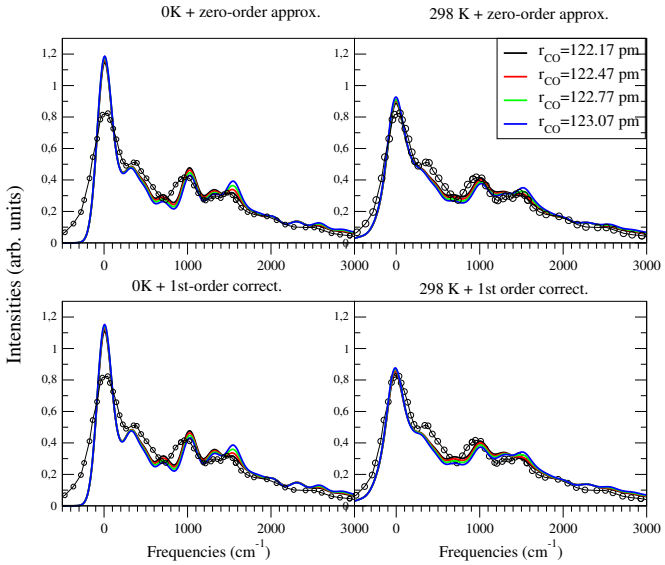

FIG. 5: Up/left(right) panel: Simulated spectra at 0K (298 K) and zero-order approximation of the dipole moment for the ^{2}A' ionized state in the region 0-3500 cm^{-1} obtained with model I for different r_{CO} distances. Bottom/left(right) panel: Simulated spectra at 0K (298K) and 1st -order approximation of the dipole moment of the ^{2}A' ionized state in the region 0-3500 cm^{-1} obtained with model I for different r_{CO} distances.

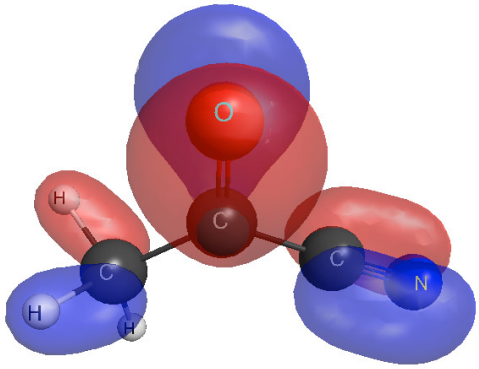

FIG. 6: Electronic density of the (out-of-plane) singly occupied Molecular orbital (HOMO-1, 3a") in acetyl cyanide

B. Band 3a"$^{(-1)}$: spectral assignments

As reported by Katsumata et al. [31] (or Fig. S1 in supporting information, I) the second band presents a broad (the fullwidth at half maximum (FWHM) ≈0.5 eV) and asymmetric profile with any clear identified structures. The tail of the peak in the high energy region clearly overlaps with the third sharp peak for which the maximum is measured at 13.82 eV.

Usually the lack of discrete vibrational structures in photoelectron spectra is indicative of a bond breaking. The width of the FC profile associated to a dissociative behavior is mainly related with the energy derivative (at the neutral equilibrium geometry) along the deformation implying one or few vibrational modes.

Here, the geometry optimization leads to a bound state where the bond lengths and angles corresponding to the DFT/B3LYP 3a"$^{(-1)}$ optimized geometry reported in Table I (right panel) does not reveal any bond cleavage.

However, obviously the Cs molecular symmetry is held, few characteristic changes in the new equilibrium geometry compared to the neutral state are significant. The free zero-point vibrational (ΔZPE) energy difference between

the adiabatic electronic energy of the 3a"$^{-1}$ cationic state in its fully optimized geometry and the neutral geometry indicates a substantially larger (-0.26 eV or 2100 cm^{-1}) gain of energy due to nuclear relaxation compared to the adiabatic 15a'$^{-1}$ cationic final state. As it can be seen in Fig.6, the electronic density on 3a" molecular orbital (HOMO) is mostly localized on C=O and C≡N moieties as well as on the two CH bonds located out of the molecular plane. The maximum bond displacement amounts to +0.088 Å with a net lengthening of the C=O bond distance and a large shortening of the r(C_2-C_3) and r(C_1-C_2) chemical bonds by ≈-0.050 Å.

As an unexpected result these structural changes are accompanied by rotation (60 degrees) of the methyl group around the C_1-C_2 chemical bond. Within such conditions the C_1H_8 bond moves in the molecular plane while C_1H_7 and C_1H_6 move out of the molecular plane. As displayed in Table I the C_1H_8 bond length (1.084 Å) is not significantly modified compared to the C_1H_6 (1.086 Å) distance recorded in the neutral electronic ground state. Concomitantly the out-of-plane CH bonds increase (1.11 Å) compared to the value in the initial neutral state ($C_1H_{7,8}$ =1.092 Å). Meanwhile, the large increase of the C=O bond and in a less extent of the C≡N bond lead to a net reduction by 600 cm^{-1} (1115 cm^{-1} vs 1776 cm^{-1}) and 100 cm^{-1} (2207 cm^{-1} vs 2323 cm^{-1}) of the corresponding ω_{CO} and ω_{CN} stretching frequencies for the 3a"$^{(-1)}$ state.

The simulation of the FC profile for the 3a"$^{(-1)}$ state is not as straightforward as for the 15a'$^{(-1)}$ state due to this specific rotation of the methyl group. The reason is that the calculations are performed considering normal coordinates expressed in terms of Cartesian displacements. This means that bending deformation, although largely determinant for activation of the angular deformation modes, also artificially activates the stretching modes. One can thus anticipate that the model, successfully applied for the 15a'$^{(-1)}$ state, will fail here to reproduce the experimental profile where rotation of the methyl group will fortuitously activate the CH stretching modes with high frequencies. Moreover, due to rotational motion, the bijective relationships between the normal modes in the initial state and in the final state becomes here clearly more ambiguous.
To prove these statements, in Table V we have reported the projections of each normal mode Q"$_k$($k = 1, 18$) onto the eighteen Q_k($k = 1, 18$) normal modes of the initial state. Except for $\omega"_{12,17,11}$ and $\omega"_3$, each mode in the final state is built over a large number of normal modes of the electronic ground state. This is particularly true for the $\omega"_{18}$ mode at 142 cm^{-1} (see Fig7) where the values of the projections onto the methyl torsion mode ω_{18} (0.23) or the modes ω_{17} (0.12) are rather weak while an unexpected large projection (0.46) is found for the symmetric stretching mode ω_2 of the methyl group. This description is in contradiction with a graphical animation (not shown here) and Fig.7 where the $\omega"_{18}$ mode mainly corresponds to the cooperative torsion of the CH_3 methyl group combined with the out-of-plane C-CN bending motion. Conversely (see Table V), the projection of $\omega"_1$ on the symmetric stretching mode of the methyl group (ω_2) is surprisingly weak (0.24) while a large projection (0.46) is found for the ω_{18} mode.

Due to the rotation of the methyl group the coupling between torsion and stretching modes is clearly purely fortuitous and biases the calculation of the Franck-Condon factors. In order to circumvent the problem raised by rotation of the methyl group, we computed in a first step the Franck-Condon factors for the mode $\omega"_{18}$ where the methyl group is really rotated by 60 degrees in the final state compared to the initial geometry. Using eq.18 the largest Franck-Condon factor for $\omega"_{18}$ (see table VI) is thus estimated to the fourth/fifth overtones of $\omega"_{18}$ (≈570 cm^{-1}). Obviously the cationic character of the final state compared to the (neutral) initial state this value is reliable with the rotational barrier regarding the energy difference (Δ) between the initial neutral geometry of acetyl-cyanide and its conformation where the methyl group is authorized to rotate by sixty degrees while the rest of the molecule is kept fixed in its initial coordinates. Δ is estimated to 365 cm^{-1} (4.36 kJ/mole) in reasonable agreement with the experimental rotational barrier (5.06 kJ/mole or 420 cm^{-1}[55]; 4.78 kJ/mole or 400 cm^{-1}[56]).

In a second step, our approach consists now to apply a reverse rotation by -60 degrees around the C_1-C_2 bond axis in order to align the CH bonds between the initial and final states. We thus recomputed (i) the components of the normal coordinates in the sub-space formed by the three hydrogens and (ii) derived the Franck-Condon factors with the new hydrogen cartesian coordinates. For each mode nine new components are thus introduced into the normal modes of the 3a"$^{(-1)}$ final state where the condition of normalization through eq.6 is fulfilled with the new set of $\alpha_{l,j}$ components (see eq.5). As a results, with the transformed normal modes induced by the methyl rotation (60^o) the projection of $\omega"_{18}$ onto the initial ω_{18} torsion mode is now estimated to 0.78 instead of 0.23 while the projection value onto the out-of-plane C-CN bending mode is still equal to 0.12. It can also be noticed that thanks to our approach the largest Franck-Condon factor associated to the C-H stretching modes corresponds to the 0→0 transition in expected accordance with the small change of the CH bond lengths.

As for the 3a"$^{(-1)}$ electronic state we have considered different levels of approximations (bijective/surjective/temperature effects) for calculation of the Franck-Condon factors, ignoring here high (1st,2nd) order corrections of the dipole moment. First the ionization energy (IE) without zero-point energy (ZPE) correction was estimated for the 3a"$^{(-1)}$ final state at DFT/B3LYP level of theory.

The corresponding IE is equal to 12.556 eV. Considering the zero-point energy corrections for the neutral and the final states, AIE(0→0) is finally estimated to 12.446 eV. In spite, as seen for the 15a' state, the DFT value is slightly underestimated with respect to measurement, it significantly differs (≈-0.6 eV) with the (vertical) experimental energy position of the maximum (13.09 eV) associated with the band 3a", suggesting here excitation of a reasonable number of quantum vibrational levels. The Franck-Condon factors reported in Table VI clearly

TABLE V: Horizontally: Calculated DFT/B3LYP/cc-pCVQZ frequencies of the harmonic vibrational modes (ω_i, i=1-18) of the initial ground state; vertically: Calculated DFT/B3LYP frequencies of the harmonic vibrational modes (ω'_i, i=1-18) of the cationic state and squared of coefficients of projection of the normal modes of the cation onto the neutral fundamental vibrational modes. In bold the largest absolute squared overlap coefficient. In parenthesis (red color) are given the largest overlap coefficient taking into account the change of the normal mode sub-space after rotation of the methyl group (see discussion in text). The modes are indexed using the Cs symmetry and decreasing frequency values (in parenthesis are given the numbering following the increasing order of frequencies).

Mode	ω	ω_{18}	ω_{12}	ω_{17}	ω_{11}	ω_{16}	ω_{10}	ω_9	ω_8	ω_{15}	ω_7	ω_6	ω_5	ω_{14}	ω_4	ω_3	ω_2	ω_{13}	ω_1
		129	177	245	437	596	599	715	985	1049	1193	1398	1458	1468	1776	2323	3031	3086	3146
$\omega"_{18}$(1)	142	**0.23** (0.78)	–	0.12 (0.12)	–(0.01)	0.02 (0.02)	–	–	(0.01)	0.01	–	0.08	–	–	–	–	**0.46** (0.00)	0.02 (0.01)	0.02 (0.01)
$\omega"_{17}$ (3)	209	0.04 (0.11)	–	**0.85** (0.84)	–	0.02	–	–	–	0.01	–	0.01	–	–	–	–	0.06	–	–
$\omega"_{16}$ (5)	529	0.02	–	–	0.02	**0.68** (0.62)	0.01	0.02	**0.10** (0.11)	0.01	0.03	–	0.02	0.01	–	–	0.03	0.02	0.03
$\omega"_{15}$ (8)	899	–	–	–	0.02	0.07	0.01	0.01	0.09 (0.13)	**0.58** (0.55)	0.08 (0.07)	–	0.01	–	–	–	0.02	0.06	0.05
$\omega"_{14}$ (13)	1309	0.01	–	–	0.01	–	–	0.01	0.03	–	0.01	0.01	**0.40** (0.63)	0.03 (0.28)	0.01	–	0.02	**0.42** (0.00)	0.04
$\omega"_{13}$ (16)	2851	0.02	–	–	0.01	0.01	–	–	0.04	0.06	0.03	–	**0.13** (0.02)	**0.34** (0.00)	–	–	–	0.07 (0.29)	**0.28** (0.58)
$\omega"_{12}$ (2)	174	–	**0.95** (0.90)	–	0.02	–	–	–	–	–	–	–	–	–	–	0.01	–	–	–
$\omega"_{11}$ (4)	399	–	0.01	0.01	**0.83** (0.72)	0.02	0.03	0.03	–	0.03	0.01	–	–	0.01	–	–	–	0.01	0.01
$\omega"_{10}$ (6)	580	–	–	–	0.05	–	**0.73** (0.73)	**0.14** (0.14)	0.05	–	–	–	–	–	0.01	0.02	–	–	–
$\omega"_{9}$ (7)	711	–	0.01	–	0.03	0.02	**0.19** (0.18)	**0.64** (0.63)	–	0.03	–	–	–	0.01	0.03	–	0.01	0.01	0.02
$\omega"_{8}$ (9)	927	–	–	–	–	0.03	0.01	**0.13** (0.14)	**0.36** (0.35)	0.05	–	–	0.01	0.01	**0.35** (0.36)	–	0.01	0.02	0.02
$\omega"_{7}$(10)	1115	0.01	–	–	–	0.02	–	0.01	0.06	0.07 (0.11)	**0.21** (0.20)	0.03	0.01 (0.11)	0.02	**0.31** (0.28)	–	0.02	0.08	**0.16** (0.00)
$\omega"_{6}$(11)	1213	0.04	–	–	0.01	0.03	0.01	–	–	0.04	0.08	**0.22** (0.22)	0.02 (0.19)	**0.34** (0.37)	0.04	–	–	0.01	**0.14** (0.00)
$\omega"_{5}$ (12)	1290	0.01	–	–	–	0.01	0.01	–	**0.21** (0.20)	–	**0.46** (0.48)	0.02	0.01	0.03	**0.21**(0.23)	–	–	0.01	0.01
$\omega"_{4}$ (14)	1454	0.05	–	–	–	0.01	–	–	0.01	0.02	0.05	**0.57** (0.69)	0.01	**0.14** (0.20)	0.02	–	0.02	0.06	0.04
$\omega"_{3}$ (15)	2207	–	0.01	0.01	–	–	0.01	–	–	–	0.01	–	–	–	0.01	**0.95** (0.96)	–	–	–
$\omega"_{2}$ (17)	2868	**0.46** (0.00)	–	–	–	0.01	–	–	0.01	0.01	0.01	–	**0.10**	0.02	–	–	**0.24** (0.69)	0.02 (0.10)	**0.10** (0.18)
$\omega"_{1}$ (18)	3167	**0.11** (0.00)	–	–	–	0.02	–	–	0.02	0.07	0.02	0.06	**0.29** (0.00)	0.03	–	–	0.10 (0.26)	**0.19** (0.49)	0.07 (0.16)

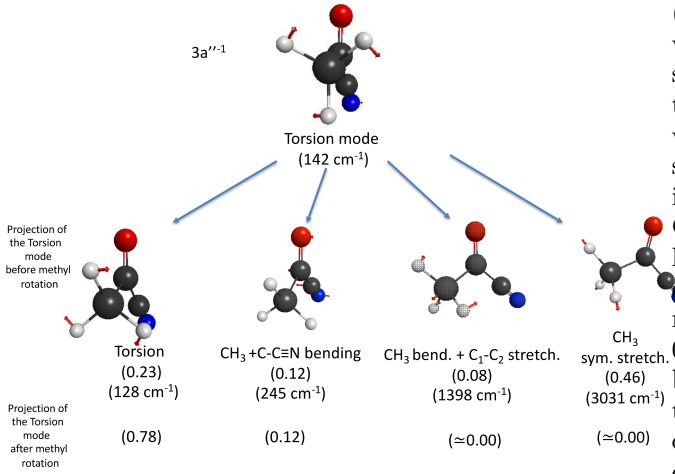

FIG. 7: top: torsion mode in the 3a"$^{(-1)}$ final state. Bottom: most important vibrational modes of the initial neutral state contributing to the linear decomposition of the 3a" torsion mode in the adiabatic geometry of the final state. In parenthesis are given the nature and corresponding projection values. Most important vibrational modes of the initial neutral state contributing to the linear decomposition of the 3a" torsion mode in the geometry after rotation by sixty degrees of the methyl group around C_1-C_2.

reveal that if the vibrational profile depend on the combination of overtones for the $\omega"_{12,10,9,15,7,6}$ modes, the vibrational progression can be largely determined by activation of the torsion mode ($\omega"_{18}$), C-C≡N bending motion ($\omega"_{12}$) and CH_3 bend+C=O stretching mode ($\omega"_7$) with frequencies at 142 cm^{-1}, 174 cm^{-1} and 1115 cm^{-1} respectively. The participation of $\omega"_7$ is not surprising since in addition to the rotation of the methyl group, the carbonyl bond length increases significantly (+0.08 Å) while the CC distances are reduced by more than 0.05 Å when removing one electron from the the 3a" molecular orbital.

A one-dimensional (3N-6/1D) bijective correspondence (see Fig.8, left panel) between (two) modes k and k" for which $\alpha_{k,k"}$ takes the largest value has been first considered. In order to evaluate the impact of the FC distribution of $\omega"_{18}$ and $\omega"_7$ onto the vibrational profile we considered two different values of S"$_{18}$ for the torsion mode, namely S"$_{18}$=0 and S"$_{18}$ =4.62. Considering S"$_{18}$=0 (see Fig.8, red line) in spite an experimental Gaussian broadening of 25 meV applied to the theoretical lines, the simulated profile exhibits well-separated bands distant by ≈1100 cm^{-1} (0.14 eV). Their energy positions roughly correspond to the fundamental (0→0) and four 0→1-4 overtones of the $\omega"_7$ mode. For each individual band a collection of transitions can be observed where the fundamental (v=0) and few overtones ($\omega"_{12}$, v=1,2) of mode 12 mostly contribute to the signal (for additional details, see supporting information, II).

Introducing the real value of S"$_{18}$, i.e. 4.62 (see Fig.8, solid green line) derived from eq.19 the spectrum becomes structureless due to the activation of a large number of overtones of the $\omega"_{18}$ torsion mode at low frequency (146 cm^{-1}) and a fairly good agreement is finally reached between theory and experiments.

If the envelope experiences a positive shift (0.07 eV) with respect to AIE due to activation of the harmonics of the $\omega"_{18}$ torsional mode the maximum of the peak (12.72 eV) is still slightly underestimated with the experimental value (13.09 eV). This is not surprising since as already seen for 15a'$^{(-1)}$ the calculated DFT IP value experiences a large red-shift (≈-0.3 eV) compared to the experimental value. By reporting an offset of 0.37 eV to our theoretical profile the maximum of the peak is found at 13.1 eV in good agreement with the experimental value.

As an interesting point that can also be raised, the theoretical bandwidth (0.4 eV) is somewhat underestimated compared to the experimental value (≈0.50 eV). The reason(s) of such discrepancy may have few different origins. For that, we have considered the surjective model considering that the S" coupling constants are each represented by a full (3N-6 x 3N-6) square matrix (here N is

the total number of atoms in the molecule). In principle this approach takes into account full normalization conditions between the normal modes in the initial state and in the final state. However, the price to pay is that this approach is undeniably more greedy in computing time since it requires to consider numerous terms as described in eq.8. Temperature effect was here fully neglected.

The simulated spectrum (see Fig.9, left panel, green color) is found slightly different compared to the one obtained with the bijective approach (blue color). In particular the double peak structure of the maximum is modified where a net shift of the FC distribution operates towards the 0→1 transition associated to mode $\omega"_7$. This effect can be explained by the fact that the $\omega"_7$ mode projects over four different modes ($\omega_{15}/\omega_7/\omega_5/\omega_4$) of the initial state, the intensities being thus strongly dependent of interference effects inherent to the surjective approach.

As for the previous 15a' electronic state, small errors on the coupling constant values or temperature effects may also play a role onto the final shape of the vibrational profile. We have considered several reasonable values of RS"$_7$ (-1.0/-1.1/-1.3/-1.4/-1.5) around the theoretical value (-1.198, see Table VI) for the mode $\omega"_7$ which mostly contributes to the vibrational profile. The simulated spectra are reported in Fig.9 either ignoring (middle panel dashed lines) or including (right panel solid lines) temperature. As expected, changing the value of RS"$_7$ sensibly modifies the Franck-Condon distribution. Among the different values considered here of the coupling constant the determination of the optimal RS"$_7$ value is rather difficult, since the accurate simulation of the high binding energy region of the spectrum is hindered because the overlap between the second and the third bands. However, the best agreement seems to be for RS"$_7$=-1.3 where the shape is pretty well reproduced and the maximum of the peak (13.18 eV) is found close to that observed experimentally (≈13.15 eV). Introducing temperature effects within a bijective approach, the theoretical profile is also slightly modified due to contribution of the hot bands and the theoretical full width at half maximum (FWHM) of the band increases to reach a value close to 0.45 eV in rather well agreement with experiments. Working at low temperature could be essential to capture the vibrational distribution associated to $\omega"_7$.

IV. INFRA-RED SPECTRA: NEUTRAL, 15A'$^{(-1)}$ AND 3A"$^{(-1)}$ STATES

In Fig.10 (upper panel) we have reported the calculated (DFT/B3LYP) infra-red (IR) spectrum of acetylcyanide in its neutral electronic ground state covering a 0-3500 cm^{-1} frequency domain. As observed experimentally [40] the IR spectrum is dominated in the region 1000-2500 cm^{-1} by two bands centered at 1193 cm^{-1} and 1776 cm^{-1} and respectively assigned to the 0→1 transitions for the ω_7 (CC-stretch/C-C=O-bend/CH_3-rock) and the ω_4 (stretching C=O) vibrational modes. As stated before, the corresponding harmonic frequencies are slightly overestimated by nearly 2% with respect to the experimental values recorded at 1178 cm^{-1} and

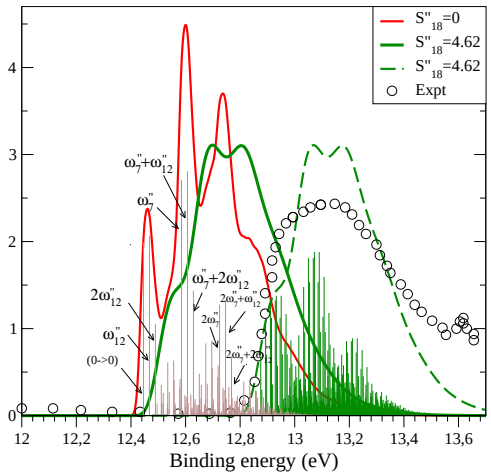

FIG. 8: 3a"$^{(-1)}$ spectrum simulated with model I (bijective) ignoring torsion coupling constant (S"$_{18}$=0, solid red line) and including torsion coupling constant (S"$_{18}$=4.62, solid and dashed green lines) values. Dashed green lines: Positive offset of 0.37 eV is applied to the green solid line spectrum. Green bars: theoretical Franck-Condon bares for the 3a"$^{(-1)}$ electronic state. Experimental broadening is fixed to 25 meV. For S"$_{18}$=0, the most important transitions ($\omega"_7$(0,1,2,3) and $\omega"_{12}$(0,1,2) in brown) are reported in the figure. For the full assignments, see supporting information, II

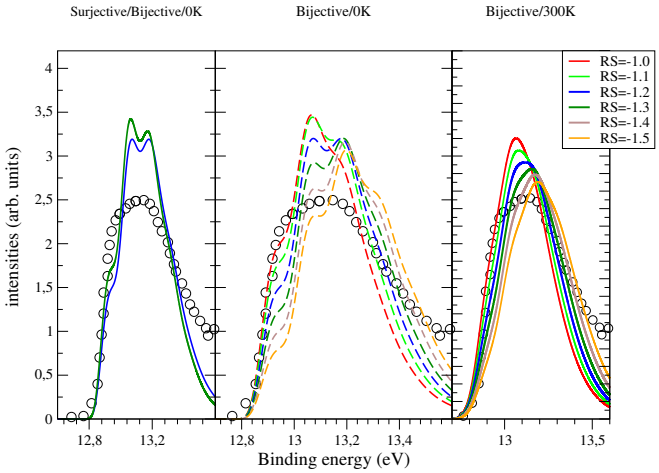

FIG. 9: Left panel: 3a"$^{(-1)}$ theoretical spectra simulated with model I (bijective, blue color) and II (surjective, green color) including torsion coupling constant S"$_{18}$=4.62 and 25 meV of experimental broadening are compared to the experimental data[31]. Middle (Right) panels: 3a"$^{(-1)}$ theoretical spectrum simulated with (bijective) model I for different coupling constant RS"$_7$ (-1.0-1.1/-1.198/-1.3/-1.4/-1.5) at 0K (298K) are compared to the experimental data[31]. Area under the theoretical and experimental peaks are identical.

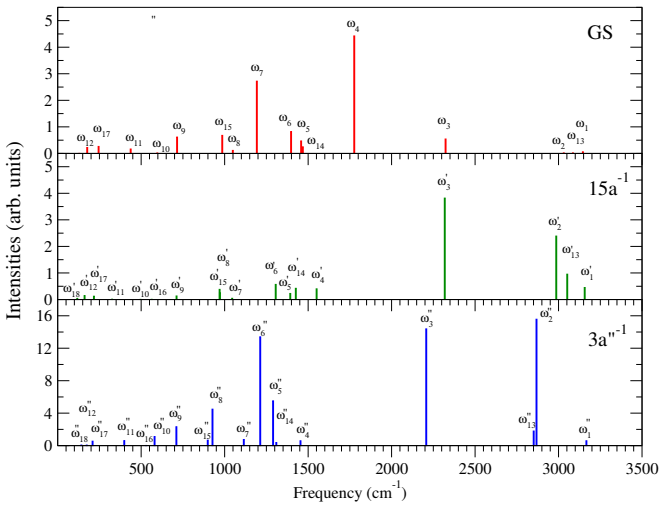

FIG. 10: Infra-red (IR) spectra the acetyl cyanide molecule in its fundamental electronic ground state (upper panel) and its cationic 15a'$^{(-1)}$ (middle panel) and 3a"$^{(-1)}$ (bottom panel) states.

1740 cm^{-1} respectively. As another feature, the intensity of the band corresponding to the fundamental transition of the mode ω_3 (stretch. C≡N) measured at 2229 cm^{-1} and calculated (harmonic approximation) at 2323 cm^{-1} is considerably reduced compared to the fundamental 0→1 excitations for the modes ω_7 and ω_4.

In Fig.10 (middle panel) is reported the theoretical Infra-red spectrum of acetyl-cyanide in the 15a'$^{(-1)}$ cationic state. It is mainly dominated by two lines, namely the fundamental 0→1 transitions for the ω'_3 (C≡N) and ω'_2 (CH_3) stretching modes. Comparing the IR and XPS spectra, the modes ω'_7 and ω'_4 at ≈1000 cm^{-1} and ≈1500 cm^{-1} mainly contributing to the satellite region in the photoelectron spectrum are weakly active in the IR spectrum.
For comparison (lower panel) we have reported the Infrared spectrum of acetyl-cyanide in the 3a"$^{(-1)}$ cationic state. The IR theoretical spectrum presents some characteristic differences compared to both the neutral and the 15a'$^{(-1)}$ cationic states. The spectrum is dominated by three bands centered at 1213 cm^{-1}, 2207 cm^{-1} and 2868 cm^{-1} corresponding to the (a') CH_3 bending (ω"$_6$) and C≡N (ω"$_3$)/CH_3 (ω"$_2$) stretching modes. The frequencies of these modes clearly differ by more than 100 cm^{-1} from the most intense lines observed in the 15a'$^{(-1)}$ IR spectrum leaving no doubt about the specific spectral signatures of the two cationic states by IR spectroscopy. The spectral region 2000-2300 cm^{-1} draws special interest from astrobiologists because the triple CN bonds of nitriles that are considered relevant to pre-biotic chemistry, fall for the neutral but considerably increases in this region for the ionized species.

V. CONCLUSION

The two low-lying bands of the valence photoelectron spectrum of the acetyl cyanide molecule in gas phase have been simulated and compared to the recorded experimental data. For that we used here an original approach using changes of geometries/frequencies/normal modes/orthonormal projection of normal modes between the initial and final states to estimate Franck-Condon factors in order to deliver accurate simulated profiles. The calculations reveal two singular profiles due to different molecular deformations. As clearly stated the vibrational profile of the photoelectron spectrum of the 15a'$^{(-1)}$ (^{2}A') ionized final state is not due solely to the CCO bending mode as claimed previously but results of activation of different modes. Essentially, it is mainly due to activation of the carbonyl group (CO) through excitations of the single overtone (v=0→v'=1) associated to the C=O stretching (1551 cm^{-1}), C-C=O bending (325 cm^{-1}, 1045 cm^{-1}), C-C=O out-of-plane wagging (496 cm^{-1}) modes, with also C-CN bending (161 cm^{-1}) motion and various bands of combination. These modes are responsible of a large vibrational progression extending up to 3500 cm^{-1} with respect to the main band with a (fortuitous) spacing between the most intense peaks of ≈500 cm^{-1}.
For the second ionized electronic state, i.e. 3a"$^{(-1)}$ (^{2}A"), the asymmetric shape of the peak is mainly due to excitations of a vibrational mode at 1115 cm^{-1} associated to C-H (CH_3) bending and C=O stretch. But the broad envelope results from rotation by sixty degrees of the CH_3 group in the adiabatic final state geometry which activates significantly the torsion mode with the lowest frequency at ≈142 cm^{-1}. The peculiar treatment of the rotational motion of methyl group responsible of the wide and structure-free vibrational profile is particularly considered. In both cases the various activated modes responsible of the Franck-Condon profiles reflect the localization of the electronic density of the corresponding electronic final states. The computed IR spectra of the two cationic states show that each of these electronic states can be easily identified. The infra-red signature of the triple CN bonds of nitriles relevant to pre-biotic chemistry is particularly exalted in both the cationic states.

VI. SUPPORTING INFORMATIONS

I: Experimental photoelectron spectrum of acetyl cyanide taken from Ref.[31]. The blue (red) arrows indicate the two regions of interest corresponding to the 15a'$^{(-1)}$ and 3a"$^{(-1)}$ final states; Recorded photoelectron spectrum of the cationic 15a'$^{(-1)}$ electronic state of acetyl cyanide taken from Ref.[31] showing the vibrational profile extended over 3500 cm^{-1}. II: Assignments of the most important vibrational bands in the satellite energy region (between 0-2000 cm^{-1}) of the 3a"$^{-1}$ photoelectron line. III: Simulations of zero-order up to second order (restricted to diagonal terms) approximation of the dipole moment of the 15a'$^{-1}$ photoelectron line. Numerical calculations of the first and second order terms of the

TABLE VI: DFT/B3LYP/cc-pCVQZ frequencies of the harmonic vibrational modes associated to the 15a'$^{(-1)}$ ionized state. RS values and diagonal ($FC_{0\to n}$(n=1-to-4)) Franck-Condon factors derived from eq.10 for model I and II (see text). In bold: most important FC factor (≥ 0.06) contributing to the vibrational profile.

Mode	Frequency	RS(k)	$FC_{0\to0}$	$FC_{0\to1}$	$FC_{0\to2}$	$FC_{0\to3}$	$FC_{0\to4}$	$FC_{0\to5}$	$FC_{0\to6}$	$FC_{0\to7}$	$FC_{0\to8}$	$FC_{0\to9}$
$\omega"_{18}$ (1)	142	-2.15	0.0078	0.0361	**0.085**	**0.1365**	**0.1672**	**0.16712**	**0.1418**	**0.1049**	**0.0691**	0.0412
$\omega"_{17}$ (3)	209	- 0.065	**0.9929**	0.0042	0.0028	0.0004	0.0001	–				
$\omega"_{16}$ (5)	529	-0.260	**0.9369**	**0.0630**	0.0003	0.0001	–	–				
$\omega"_{15}$ (8)	899	-0.454	**0.8246**	**0.1687**	0.0067	–	–	–				
$\omega"_{14}$ (13)	1309	0.270	**0.9319**	**0.0678**	0.0002	0.0001	–	–				
$\omega"_{13}$ (16)	2851	-0.091	**0.9909**	0.0082	0.0008	–	–	–				
$\omega"_{12}$ (2)	174	1.019	**0.3571**	**0.3706**	**0.1894**	**0.06352**	0.0157	0.0031				
$\omega"_{11}$ (4)	399	-0.266	**0.9339**	**0.0658**	0.0003	0.0001	–	–				
$\omega"_{10}$ (6)	580	0.362	**0.8791**	**0.1150**	0.0058	0.0001	–	–				
$\omega"_{9}$ (7)	711	0.554	**0.7365**	**0.2260**	0.0341	0.0032	0.0002	–				
$\omega"_{8}$ (9)	927	-0.229	**0.9501**	0.0497	0.0002	0.0001	–	–				
$\omega"_{7}$ (10)	1115	-1.198	**0.3218**	**0.4377**	**0.2060**	0.0331	0.0003	–				
$\omega"_{6}$ (11)	1213	0.345	**0.8939**	**0.10539**	0.0002	0.0005	–	–				
$\omega"_{5}$ (12)	1290	-0.205	**0.9565**	0.0401	0.0031	0.0002	–	–				
$\omega"_{4}$ (14)	1454	-0.064	**0.9956**	0.00412	0.0003	0.0000	–	–				
$\omega"_{3}$ (15)	2207	-0.120	**0.9857**	0.0143	0.0001	–	–	–				
$\omega"_{2}$ (17)	2868	0.010	**0.9995**	0.0004	0.0001	–	–	–				
$\omega"_{1}$ (18)	3167	0.089	**0.9919**	0.0079	0.0022	–	–	–				

dipole moments

[1] E. Herbst and E. F. van Dishoeck, *Annu. Rev. Astron. Astrophys.*, 2009 **47**, 427.

[2] https://en.wikipedia.org/wiki/List_of_interstellar_and_circumstellar_molecules

[3] K. Krumova and G. Cosa, Chapter 1: Overview of Reactive Oxygen Species , in Singlet Oxygen: Applications in Biosciences and Nanosciences, **1**, 1-21, Comprehensive Series in Photochemical and Photobiological Sciences (2016) DOI: 10.1039/9781782622208-00001

[4] D. A. Williams, T. W Hartquist, J. M. C. Rawlings, C. Cecchi-Pestellini, S. Viti, Chapter 1: Chemistry and Dynamics in the Interstellar Medium , in *Dynam. Astrochem.*, 2017, 1-20 DOI: 10.1039/9781782629894-00001

[5] Front. Astron. Space Sci., 2021 https://doi.org/10.3389/fspas.2021.776942

[6] J. Bublitz, J. Kastner 1 , P. Hily-Blant, T. Forveille, M. Santander-García, V. Bujarrabal, J. Alcolea and R. Montez, Jr., *Galax.* 2020 **8**, 32 doi:10.3390/galaxies8020032

[7] A. Hacar, A. D. Bosman and E. F. van Dishoeck, *Astron. and Astrophy.*, 2020, **635**, A4

[8] S-R Tsai and M. R. Hamblin, *J. of . Photochem. and Photobiolo.: Biology* ,2017, **170**, 197.

[9] S. L. McArthur, G. Mishra and C. D. Easton, Applications of XPS in Biology and Biointerface Analysis. In: Smentkowski, V. (eds) *Surface Analysis and Techniques in Biology*, Springer, 2014, doi.org/10.1007/978-3-319-01360-2_2

[10] D. Mayer et al., *Nat. Comm.*, 2022, **13**; https://doi.org/10.1038/s41467-021-27908-y

[11] O. Travnikova, K. J. Borve, M. Patanen, J. Söderström, C. Miron, L. J. Saethre, N. Mårtensson and S. Svensson, *J. of Elec. Spectrosc. and Rel. Phenom.*, 2012, **185**, 191.

[12] G. Greczinsky and L. Hultman, *Prog. in Mater. Sci.*, 2020, **107**, 100591.

[13] K. Siegbahn, C. Nordling, A. Fahlman, R. Nordberg, K. Hamrin, J. Hedman, G. Johansson, T. Bergmark, S.-E. Karlsson, I. Lindgren, B. Lindberg, ESCA, Atomic, Molecular and Solid State Structure Studied by Means of Electron Spectroscopy, Almqvist and Wiksells, Uppsala, 1967.

[14] Y. Oba, T. Tomaru, T. Lamberts, A. Kouchi and N. Watanabe, *Nat. Astro.*, 2018, **2**, 228

[15] S. H. Cuylle, D. Zhao, G. Strazzulla and H. Linnartz, *Astron. and Astrophys.* 2014, **570**, A83, DOI: 10.1051/0004-6361/201424379

[16] M. Accolla, G. Pellegrino, G. A. Baratta, G. G. Condorelli, G. Fedoseev, C. Sciré, M. E. Palumbo, and G. Strazzulla, *Astron. and Astroph.*, 2018,**620** A123

[17] A. Foster, R. Smith, N. Brickhouse, N., T. Kallman, and M. Witthoeft, *Space Science Reviews*, 2010, **157**, 135.

[18] T. Kallman, P. Palmeri, *Reviews of Modern Physics*, 2007, **79**, 79-133

[19] S. Lepp, S, A. Dalgarno, *Astronomy and Astrophysics*, 1996, **306**, L21-L24

[20] P. Stäuber, P.; S. Doty, E. Van Dishoeck, A. Benz, *Astronomy and Astrophysics*, 2005, **440**, 949

[21] M. Adamkovics, A.E. Glassgold, R. Meijerink, *The Astrophys. J.*, 2011, **736**, 143

[22] M. A. Baig, Atoms 10, 39.(2022) https://doi.org/10.3390/atoms10020039

[23] E.T. Kennedy, J.-P. Mosnier P. Van Kampen, D. Cubaynes, S. Guilbaud, C. Blancard, B. M. McLaughlin, and J.-M. Bizau, *Phys. Rev. A*, 2014, **90**, 063409

[24] A. Bellili, M. Schwell, Y. Bénilan, N. Fray, M.-C. Gazeau, M. Mogren Al-Mogren, J.-C. Guillemin, L. Poisson, and M. Hochlaf, *J. Chem. Phys.*, 2014, **141**, 134311

[25] A. Belloche, K. M. Menten, C. Comito, H. S. P. Müller, P. Schilke, J. Ott, S. Thorwirth and C. Hieret, *Astron. Astrophys.*, 2008, **482** 179; doi: 10.1051/0004-6361:20079203

[26] A. Strecker and A. Ueber, *Ann. Chem. Pharm.*, 1850,

75, 27
[27] C. Kahane, C. Ceccarelli, A. Faure, and E. Caux, *Astrophys. J.*, 2013, **763**, L38.
[28] A. J. Remijan, J. M. Hollis, F. J. Lovas, W. D. Stork, P. R. Jewell, and S. D. Meier, *Astrophys. J.*, 2008, **675**, L85
[29] R. J. Horwitz, J. S. Francisco, and J. A. Guest, *J. Phys. Chem. A*, 1997, **101**, 1231.
[30] J. C. Owrutsky and A. P. Baronavski, *J. Chem. Phys.*, 1999, **111**, 7329.
[31] S. Katsumata, K. Tabayashi, T. Sugihara, K. Kimura, *J. of . Elect. Spectr. and Rel. Phenom.*, 2000, **49**, 113
[32] A. Bellili, R. Linguerri, M. Hochlaf and C. Puzzarini, *J. Chem. Phys.* 2015, **143**, 184314, doi: 10.1063/1.4935493.
[33] F. Duchinsky, *Acta Physiochem. USSR*, 1937, **7**, 551
[34] A.O. Benz, S. Bruderer, E.F. Van Dishoeck, P. Staeuber, S. Wampfler, S. M. Melchior, C. Dedes, F. Wyrowski, S. Doty and F. van der Tak, *Astrono. and Astrophys.*, 2010, L35 **521**
[35] A. Tielens, *Rev. of Mod. Phys.*, 2013, **85**, 1021
[36] D. E. Woon, T. H. Dunning, *J. Chem. Phys.*, 1995, **103**, 4572, doi: 10.1063/1.470645
[37] S. Bell, G. A. Guirgis, J. Lin, J. R. Durig, *J. Mol. Struct.*, 1990, **238**, 183
[38] M. Sugie, K. Kuchitsu, *J. Mol. Struct.*, 1974, **20**, 437.
[39] C. Møller and M. S. Plesset, *Phys. Rev.*, 1934, **46**, 618.
[40] H. M. Heise, F. Scappini, and H. Dreizler, *Z. Naturforsch*, 1976, **A 31**, 1408.
[41] T. B. Adler, F. R. Manby, and H.-J. Werner, J. Chem. Phys., 2009, **130**, 054106, doi.org/10.1063/1.3040174
[42] T. B. Adler and H.-J. Werner, *J. Chem. Phys.*, 2009, **130**, 241101, doi.org/10.1063/1.3160675
[43] G. Knizia, T. B. Adler, and H.-J. Werner, *J. Chem. Phys.*, 2009, **130**, 054104, doi.org/10.1063/1.3054300
[44] 34. T. B. Adler, G. Knizia, and H.-J. Werner, *J. Chem. Phys.*, 2007,**127**, 221106, doi.org/10.1063/1.2817618
[45] A.D. Becke, *J. Chem. Phys.*, 1993, **98**, 5648.
[46] C. Lee, W. Yang, R.G. Parr, *Phys. Rev. B*, 1988, **38**, 3098.
[47] M. W. Schmidt, K. K. Baldridge, J. A. Boatz, S. T. Elbert, M. S. Gordon, J. J. Jensen, S. Koseki, N. Matsunaga, K. A. Nguyen, S. Suand, T. L. Windus, M. Dupuis and J. A. Montgomery, *J. Comput. Chem.*, 1993, **14**, 1347.
[48] T. Darrah Thomas, L. J. Saethre, S. L. Sorensen and S. Svensson, *J. Chem. Phys.*, 1998, **109**, 1041.
[49] J. Katriel, *J. Phys. B: Atom. Molec. Phys.*, 1970, **3**, 1315
[50] H. M. Heise, F. Scappini, and H. Dreizler, *Z. Naturforsch*, 1976, **A 31**, 1408, doi.org/10.1515/zna-1976-1121
[51] P. Macak, L. Yi and H. Ågren, *Chem. Phys. Lett.*, 2000, **330**, 447.
[52] A. A. El-Azhary and H. U. Suter, *J. Phys. Chem.*, 1996, **100**, 15056
[53] K. E. Riley, B. T. Op't Holt and M. K. Merz, *J. Chem. Theory Comput.*, 2007, **3** 407; doi: 10.1021/ct600185a
[54] J. S. Binkley, J. A. Pople and W. J. Hehre, *J. Am. Chem. Soc.*, 1980, **102** 939
[55] T. Schaefer, T. A. Wildman and R. Sebastian, *J. of . Mol. Struct.*, 1982, **89** 93
[56] S. Bell, G. A. Guirgis, J. Lin and J. R. Durig, *J. of . Mol. Struct.* , 1990, **238** 83